EUROPEAN ORGANIZATION FOR NUCLEAR RESEARCH

PROPOSAL

# A SEARCH FOR ANOMALOUS NEUTRINO DISAPPEARANCE AND OSCILLATORY PHENOMENA AT THE CERN-PS

DRAFT 2011

# TABLE OF CONTENTS

**1 INTRODUCTION AND MOTIVATIONS. 5**

1.1 STERILE NEUTRINOS ? 5
1.2 THE GALLIUM EXPERIMENTS WITH A MEGACURIE RADIOACTIVE SOURCE. 6
1.3 THE REACTOR (ANTI)-NEUTRINO DISAPPEARANCE ANOMALY. 8
1.4 THE MINIBOONE EXPERIMENTS. 8
1.5 CPT VIOLATIONS ? 11
1.6 COMBINED RE-ANALYSIS OF THE NEUTRINO ANOMALIES. 11
1.7 A MORE DIRECT, NEW APPROACH TO NEUTRINO OSCILLATIONS. 13
1.8 OTHER RELATED EXPERIMENTS UNDER CONSIDERATION. 16

**2 THE DEVELOPMENT AND THE OPERATION OF THE LAR TPC. 20**

2.1 PRINCIPLE OF OPERATION. 20
2.2 THE ICARUS 600 TON LAR DETECTOR. 24
*2.2.1 General description of the T600. 24*
*2.2.2 Technical description. 24*
*2.2.3 Early operation of T600 in LNGS. 30*
*2.2.4 Experimentally achieved LAr purity. 32*
*2.2.5 DAQ and recording of the signals. 34*
*2.2.6 Transport of the T600 from LNGS to CERN. 36*

**3 THE EXPERIMENTAL SETUP AT THE CERN-PS. 37**

3.1 THE CERN-PS BEAM. 37
3.2 THE "FAR" DETECTOR. 41
3.3 THE "NEAR" DETECTOR. 43

**4 SIGNAL SELECTION AND BACKGROUND REJECTION. 47**

**5 SENSITIVITY TO $\nu_E$ AND $\nu_\mu$ DISAPPEARANCE SIGNALS. 55**

**6 SENSITIVITY TO $\nu_\mu \rightarrow \nu_E$ OSCILLATIONS. 59**

**7 THE REALIZATION OF THE DETECTORS AT THE CERN/PS. 62**

7.1 GENERAL CONSIDERATIONS. 62
7.2 REFURBISHING OF THE T600 IN THE CERN-PS. 62
7.3 THE NEW "NEAR" DETECTOR. 63

**8 REFERENCES. 65**

# ABSTRACT.

The present proposal describes an experimental search of sterile neutrinos beyond the Standard Model with the CERN-PS 19.2 GeV beam and the innovative technology of imaging in ultra-pure cryogenic liquid Argon. The core of the experiment will be the now operational ICARUS T600, the largest LAr-TPC ever built, with a size of about 600 t of imaging mass. The new method is based on the drift of free electrons over 1.5 m as a function of the time, observing the true "image" of the track with a spatial resolution of the order of 3 x 3 x 1 $mm^3$. The electro negative impurities currently with the T600 correspond to an equivalent Oxygen content of the order of a several tens of ppt (parts per trillion). The LAr-TPC is also an excellent calorimeter and traversing muon events are measured by multiple scattering.

The proposal is based on two strictly identical LAr-TPC detectors observing the electron-neutrino signal in the "Far" and "Near" positions, the first of about 150 tons at 127 m from the proton target, the second one of about 600 tons placed 850 m away. This project will exploit the ICARUS T600 — now running in the underground experiment CNGS2 with neutrinos from the CERN-SPS — moved from GranSasso to the CERN "Far" position. An additional (1/4) of the T600 detector (T150) will be constructed and located in the "Near" position.

In the two positions, the radial and energy spectra of the $\nu_e$ beam are practically identical. Comparing the two detectors, in absence of oscillations, all cross sections and experimental biases cancel out and the two experimentally observed event distributions must be identical. Any difference of the event distributions at the locations of the two detectors might be attributed to the possible existence of $\nu$-oscillations, presumably due to a additional neutrino with a mixing angle $\sin^2 2\theta_{new}$ and a larger mass difference $\Delta m^2_{new}$.

The superior quality of the LAr imaging TPC — now widely demonstrated experimentally — and in particular its unique e–$\pi^0$ discrimination allows full rejection of backgrounds, offers a $\nu_e$ detection without any losses.

Two main anomalies will be explored with both $\nu$ and anti-$\nu$ focussed beams. According to first anomaly some of the $\nu_e$ ($\bar{\nu}_e$) and/or of the $\nu_\mu$ ($\bar{\nu}_\mu$) events may be converted into invisible components, leading to observation of oscillatory, distance dependent disappearance rates. In a second anomaly (following LSND and MiniBooNE observations) some distance dependent $\mu_\nu \rightarrow \nu_e$ oscillations may be observed especially in the antineutrino channel.

A total LAr mass of 750 ton and a reasonable utilization of the CERN-PS with the refurbished TT7 beam line will offer remarkable discovery potentialities, collecting a very large number of unbiased events both in the neutrino and antineutrino channels, largely adequate to settle definitely the origin of the many indications behind the $\nu$-related anomalies.

# 1 Introduction and motivations.

*1.1 Sterile neutrinos ?*

Neutrinos have been the origin of an impressive number of "surprises". The LEP experiments have demonstrated that the sum of the strengths of the coupling of different neutrinos is very close to 3, confirming a previous result by UA1. *But it is only assuming that neutrinos, in similarity to charged leptons, have unitary strengths that the resulting number of neutrinos is 3.*

Recent results have shown that a precise identity between neutrino and charged lepton families is by no means automatically granted. The recent observation of the extraordinarily large neutrino mixings when compared to naive Cabibbo-like expectations from quarks, the question of right-handed partners, the possibility of Majorana-like couplings, the extraordinary small mass spectrum and so on, leave a large number of potential features untested. The experimentally measured weak coupling strengths are only rather poorly known, leaving room for many other alternatives.

Neutrino oscillations have established a picture for a large number of experiments consistent with the mixing of three physical neutrino $\nu_e$,$\nu_\mu$ and $\nu_\tau$ with mass eigenstates $\nu_1$,$\nu_2$ and $\nu_3$ [1]. In particular the mass differences turn out to be relatively small, $\left|\Delta m^2_{31}\right| \approx 2.4 \times 10^{-3} eV^2$, and $\left|\Delta m^2_{21}\right| \approx 8 \times 10^{-5} eV^2$. There are however a number of anomalies which, if confirmed experimentally, could be due to the presence of an additional, large squared mass difference for instance in the framework of four-neutrinos with mixing. Evidently if more than the two oscillation signals were to be eventually observed, additional Physics beyond the Standard Model in the neutrino sector will be necessary.

The possible presence of sterile neutrinos has been proposed by B. Pontecorvo [2]. It has been discussed since a very long time, but so far without conclusive evidence. Two distinct classes of phenomena have been analyzed, namely a) the apparent reduction in the $\bar{\nu}_e$ detected by low energy neutrinos from nuclear reactors [3] and from the signal from Mega-Curie sources in the Gallium experiments [4] [5] originally designed to detect solar neutrino deficit [3], and b) evidence for a $\bar{\nu}_e$ excess signal of in interactions coming from neutrinos from particle accelerators [6] [7] [8].

These experiments may all point out to the possible existence of the fourth non standard neutrino state driving neutrino oscillations at a small distances, with typically $\left|\Delta m^2_{new}\right| > 1\ eV$ and relatively large mixing angle $\left|\sin^2_{new}\right| \approx 0.1$ [9].

The class a) of phenomena hint at a significant fast disappearance rate in the initial $\bar{\nu}_e$ production and the class b) predicts an anomalous

$\nu_\mu \rightarrow \nu_e$ oscillation, and with similar, large $\left|\Delta m^2_{new}\right|$ values, much greater than the ones of the Standard Model. These alternatives will be extensively explored by our presently proposed experiment with both neutrino and anti-neutrino beams from a newly designed beam from the CERN/PS.

More recently the existence of a fourth neutrino state may be also hinted — or at least not excluded — by cosmological data mainly coming from WMAP and other observations [10]. It is only because the masses of known neutrino species are so small, that their contribution to the Dark Matter of the Universe can be excluded. The situation could be altered by the additional presence of sterile neutrinos, provided they are sufficiently massive. Therefore, the presence of massive sterile neutrinos, will contribute also to clarify the Dark Matter problem.

The present experimental proposal is designed to clarify directly — in the above mentioned range of values for $\left|\Delta m^2_{new}\right|$ and mixing angles — the existence of a fourth non standard neutrino state. The proposal is based on two strictly identical LAr-TPC detectors [11] observing the electron-neutrino signal in the "Near" and "Far" positions, the first of about 150 tons at 127 m from the proton target, the second one of about 600 tons placed 850 m away [12]. In this way, all cross sections and experimental biases cancel out. In absence of oscillations the two experimentally observed event distributions must be identical, the background electron neutrino radial and energy distributions being extremely similar in the two positions. Any difference of the event distributions due to the position between the two detectors should be attributed to the possible existence of oscillations, determining separately both the mixing angle $\left|\sin^2_{new}\right|$ and the mass difference $\left|\Delta m^2_{new}\right|$.

*1.2 The Gallium experiments with a MegaCurie radioactive source.*

In the late nineties the SAGE [4] and GALLEX [5] experiments, designed to determine neutrino signal from the Sun, also recorded the $\nu_e$ calibration signal produced by intense artificial k-capture sources of $^{51}Cr$ and $^{37}Ar$ placed at a very short distance from the detector. The averaged result of the ratio R between the source detected and produced neutrino rates are consistent with each other, $R = 0.86^{+0.05}_{-0.05}$ but about 2.7 σ away from the R = 1 expectation. The result is somewhat influenced by uncertainties in the nuclear models, which however they may not be enough to bring R to unity [13]. Best fitted values may favour the existence of an undetected sterile neutrino with an evidence of 2.3 σ with a broad range of values centred around $\left|\Delta m^2_{new}\right| \approx 2\ eV^2$ and $\left|\sin^2_{new}\right| \approx 0.3$ [3] [9].

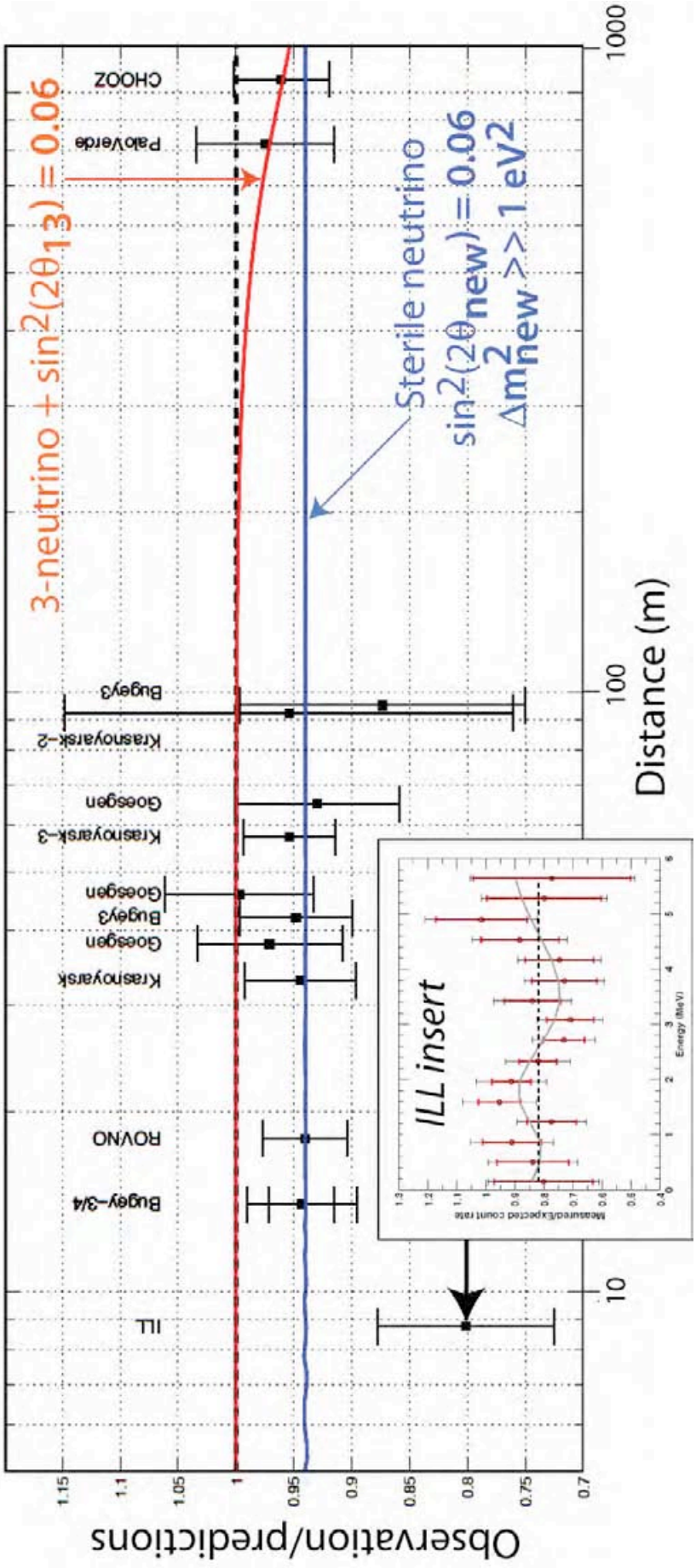


**Figure 1**-. From Ref. [3]. Illustration of the short baseline reactor antineutrino anomaly. The experimental results are compared to the prediction without oscillation, taking into account the new antineutrino spectra, the corrections of the neutron mean lifetime, and the off-equilibrium effects. Published experimental errors and antineutrino spectra errors are added in quadrature. The mean averaged ratio including possible correlations is 0.937 ± 0.027. The red line shows a 3 active neutrino mixing solution fitting the data, with $sin^2(2\theta_{13}) = 0.06$. The blue line displays a solution including a new neutrino mass state, such as $\Delta m^2_{new} \gg 1$ eV$^2$ (for illustration) and $sin^2(2\theta_{new}) = 0.16$.

*1.3 The reactor (anti)-neutrino disappearance anomaly.*

Recently a re-evaluation of all the reactor antineutrino spectra has increased the flux by about 3% [3]. With such a new flux evaluation, the ratio R between the observed and predicted rates is decreased to $R = 0.937 \pm 0.027$, leading to a deviation of 2.3 σ from unity (98.4 % confidence level) (Figure 1). However, reactor experiments all explore oscillation regions which are far away from the perspective oscillatory value of $|\Delta m^2_{new}|$, with perhaps the exception of the ILL experiment (at ≈ 9 m) which had unfortunately a very modest statistical impact (68% confidence level). The disappearance rate is given by the well known formula

$$R = 1 - \sin^2\left(2\theta^2_{new}\right)\sin^2\left(1.27\frac{\Delta m^2_{new}\left[eV^2\right]L[m]}{E_{\nu e}[MeV]}\right)$$

Assuming for instance $|\Delta m^2_{new}| = 2.0\ eV^2$ and $E_{\nu e} = 2\ MeV$, the first minimum of R occurs at L = 1.236 m (for $\sin^2(\pi/2)$) and the full pattern repeats each L = 2.47 m. The actual oscillatory pattern may be somewhat washed out by the dimensions of the reactor core and by the energy resolution of the detector after a reasonably short flight-path distance from the reactor core.

*1.4 The MiniBooNE experiments.*

The MiniBooNE experiment [7] used a horn focused neutrino beam from 8 GeV protons of the FNAL Booster. The experiment had been designed to verify the observation of an anomaly by the previous LNSD experiment [6] in which $\bar{\nu}_e + p \rightarrow e^+ + n$ interactions in excess of the expected contributions due to $\bar{\nu}_e$ production have been detected. The anomalous LSND signal (87.9 ± 22.4 ± 6.0) represented a 3.8 σ effect for L/E distances of about 0.5 – 1.0 m/MeV. As well known, explaining this LNSD signal with neutrino oscillations would imply an additional mass-squared difference largely in excess of the Standard Model's values.

Data have been collected with an initial beam of $\nu_\mu$ neutrinos [7] and more recently with $\bar{\nu}_\mu$, presently continuing [8]. The 450 ton liquid scintillator detector was exposed at a ~ 0.7 GeV neutrino beam at 550 m from the target for $\nu_\mu$ with an integrated intensity of 6.6 $10^{20}$ POT (protons on target) and for $\bar{\nu}_\mu$ with 5.66 $10^{20}$ POT. While the LSND like anomaly seems to be absent in the neutrino data, a new "anomaly" appears at much smaller values of the neutrino energy (Figure 2a). A possible explanation has been described in Ref. [9], taking into account that the overall normalization factors of the $\nu_e$-induced events and of the misidentified $\nu_\mu$ events are as large as $f_\nu = 1.21 \pm 0.24$.

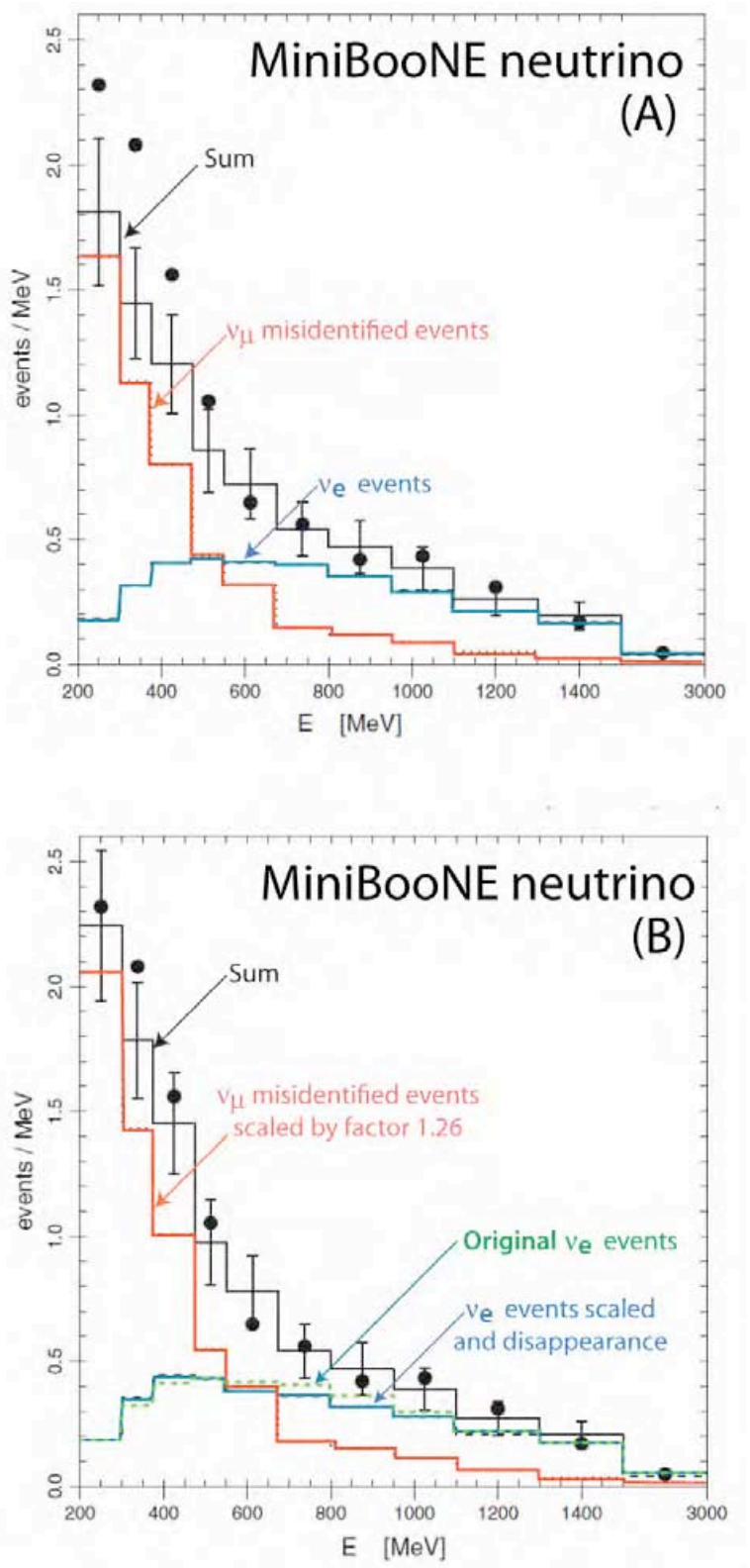


**Figure 2.** (a) MiniBooNE electron-like neutrino data. Comparison between the data (black dots) and the calculated distributions due to misidentified **νμ** events (red) and genuine **νe** events (blue). The sum is indicated in black. One notices an anomaly at low energies, which is incompatible with LNSD predictions. (b) according to Ref. [9] scaling of the events is applied with a factor 1.26, within the permitted uncertainty of $f_\nu = 1.21 \pm 0.24$ and gives an acceptable fit to the data. The νe with and without scaling and disappearance are also shown.

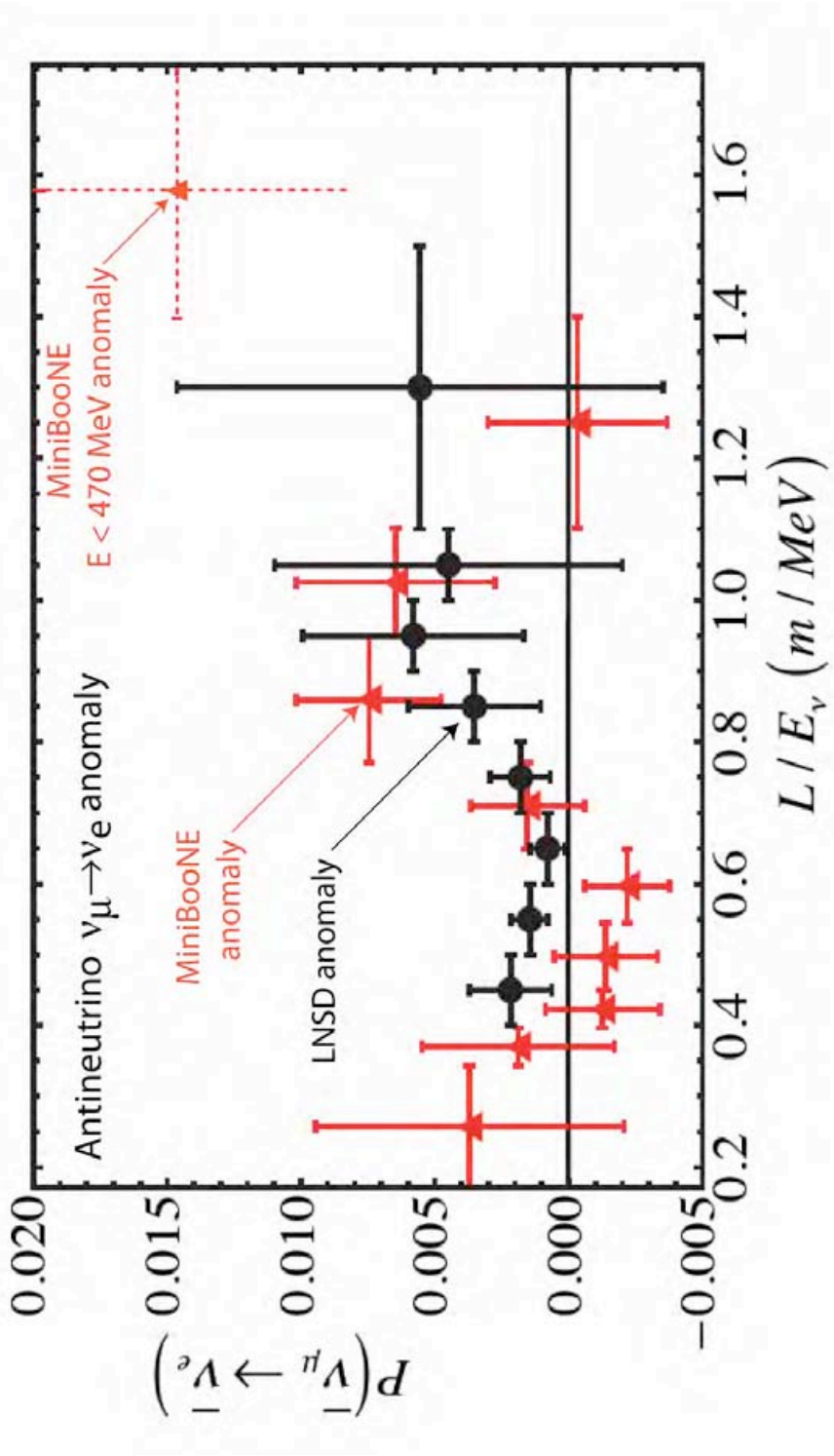


**Figure 3.-** The more recent MiniBooNE antineutrino run [8] shows the direct presence of a LSND like anomaly [8] for neutrino energies > 430 MeV. The result is compelling with respect to the ordinary two-neutrino fit, indicating a 99.4% probability for an anomalous excess in $\nu_e$ production. The reported $\nu_\mu$ effect is also broadly compatible with the expectation of LNSD experiment, which, as well known, was originally dominant in the antineutrino channel

Such a scaling factor applied to the misidentified $\nu_\mu$ events which are dominant at E ≤ 430 MeV can effectively nullify the anomaly (Figure 2b). The sum spectrum, in which also the $\nu_e$ events are included, is perfectly consistent with the $\nu_e$ disappearance rate for a broad interval of values around the previously indicated predictions for $|\Delta m^2_{new}|$ and for $|\sin^2_{new}|$ of Gallium and Reactor experiments, although with a very weak statistical evidence, as evident comparing the $\nu_e$ spectra of Figure 2b.

The more recent MiniBooNE antineutrino run [8] shows however the direct presence of a LSND like $\bar{\nu}_\mu \rightarrow \bar{\nu}_e$ anomaly for neutrino energies > 430 MeV. The result is compelling with respect to the ordinary two-neutrino fit, indicating a 99.4% probability for an anomalous excess in $\bar{\nu}_e$ production. The reported $\bar{\nu}_\mu$ effect is also broadly compatible with the expectation of LNSD experiment, which, as well known, was originally dominant in the antineutrino channel (Figure 3). This anomaly — of course completely different from the claimed disappearance rate in the $\bar{\nu}_e$ channel — may indicate a more complex physics situation. It may be a not negligible contribution of the type $|U_{\mu 4}|$ due to additional oscillations in the direct channel $\bar{\nu}_\mu \rightarrow \bar{\nu}_e$ or some other unknown mechanism. The antineutrino MiniBooNE exposure at the FNAL-Booster is presently being continued until at least mid 2011. The presently proposed experiment — because of the much higher resolution of the LAr-TPC, identifying unambiguously the different decay channels — should definitively clarify the LNSD/MiniBooNE anomaly.

*1.5 CPT violations ?*

The "tension" between the neutrino and antineutrino MiniBooNE + LNSD data seems to indicate a difference of the effective mixing angles in the neutrino and antineutrino channels. Such a difference, if confirmed for instance by the presently proposed experiment, could be due to some unknown mechanism, or perhaps even to CPT violation. It should be pointed out that the the MINOS experiment has recently pointed out a possible difference (at about 2 σ) between the effective mixing of neutrinos and antineutrinos in the long-baseline $\nu_\mu$ and $\bar{\nu}_\mu$ disappearance channels [14].

*1.6 Combined re-analysis of the neutrino anomalies.*

The main confirmed evidence for the anomaly [3] [9] presently rests today on the missing neutrino electron yield of the reactor and Gallium experiments. Since the oscillatory behaviours is very poorly measured there is only an effective lower limit of a few eV on the value of $\Delta m^2_{new}$. In particular the Tritium data are practically irrelevant for the determination of $\sin^2(2\theta_{new})$.

The significance of the sterile neutrino oscillation hypothesis is also detailed in Table 1 from Ref. [3].

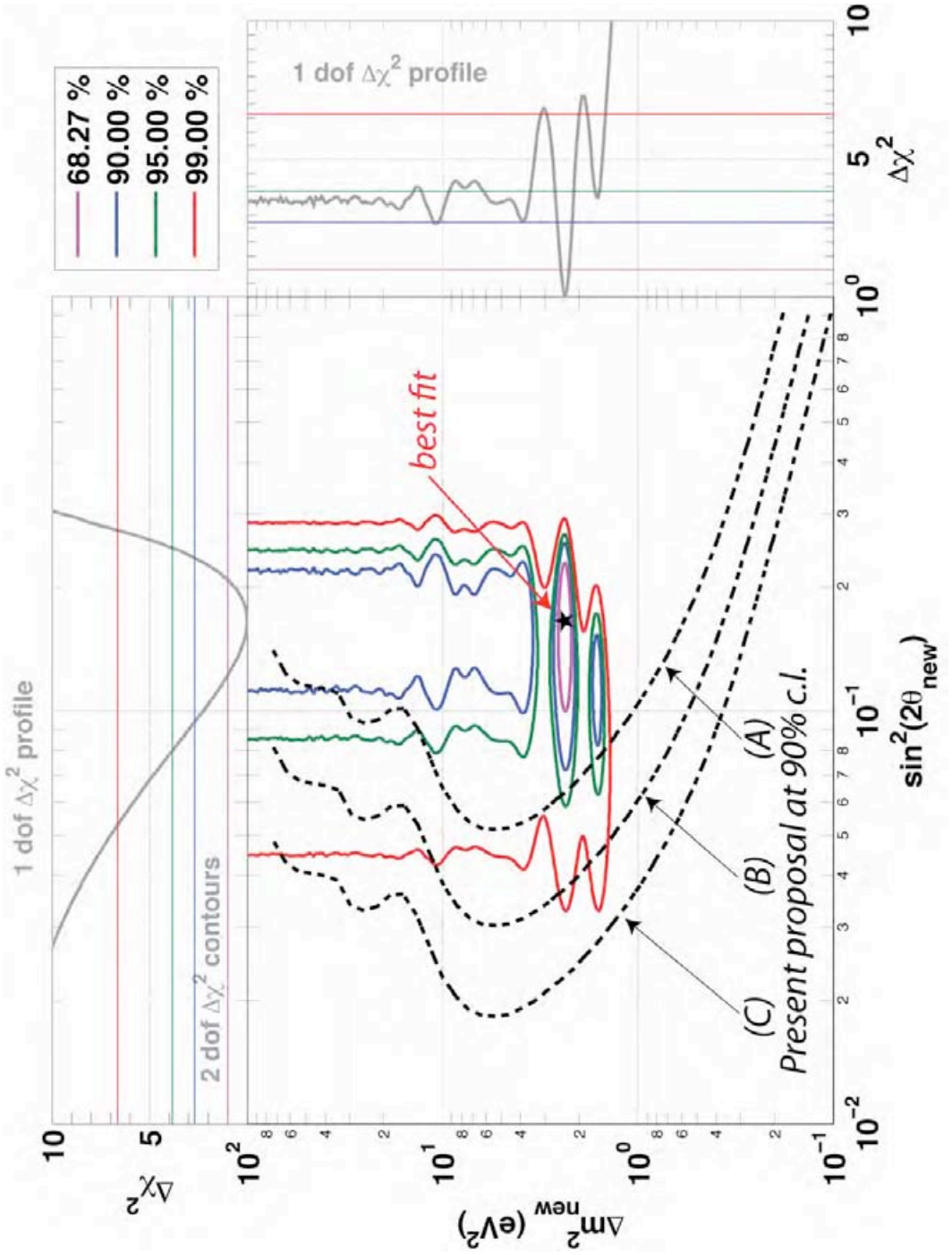


**Figure 4.-** Allowed regions in the $|\sin^2_{new}| - |\Delta m^2_{new}|$ plane for a sterile neutrino hypothesis from the combination of reactor neutrino experiments, Gallex and Sage calibration sources experiments, MiniBooNE reanalysis according to Ref. [9], and the ILL-energy spectrum distortion of Ref. [3]. Data are well fitted by the 3 + 1 neutrino hypothesis, while the no-oscillation hypothesis is disfavored at 99.93% C.L. the expected sensitivity for the presently proposed experiment is also shown as a comparison. The integrated intensity correspond to (a) 2.5 x $10^{10}$ POT (protons on target) for the original beam intensity of about 30 kWatt of the previous CERN/PS experiments, (b) to 7.5 x $10^{10}$ POT for the newly planned 90 kWatt neutrino beam at CERN/PS and (c) to an hypothetical 270 kWatt neutrino beam.

***Table 1***. *Best-fit limits and significance of the sterile neutrino hypothesis [3].*

| ***Experiment(s)*** | $\sin^2(2\theta_{new})$ | $\Delta m^2_{new}$ ***eV²*** | ***C.L.*** |
|---|---|---|---|
| Reactors (no ILL-S,R[1]) | 0.02-0.23 | $> 0.2$ | 95.0 |
| Gallium (G) | 0.06-0.4 | $> 0.3$ | 97.7 |
| MiniBooNE[2] (M) | — | — | 72.4 |
| ILL-S | — | — | 68.2 |
| R_ + G | 0.07-0.24 | $> 1.5$ | 99.7 |
| R_ + M | 0.04-0.23 | $> 1.4$ | 97.5 |
| R_ + ILL-S | 0.04-0.23 | $> 2.0$ | 97.1 |
| ALL | 0.06-0.25 | $> 2.0$ | 99.93 |

In Figure 4 are shown the allowed regions in the $|\sin^2_{new}| - |\Delta m^2_{new}|$ plane for a sterile neutrino hypothesis from the combination of reactor neutrino experiments, Gallex and Sage calibration sources experiments, MiniBooNE reanalysis according to Ref. [9], and the ILL-energy spectrum distortion [3]. Data are well fitted by the 3 + 1 neutrino hypothesis, while the no-oscillation hypothesis is disfavored at 99.93% C.L. The marginal $\Delta\chi^2$ profiles for $|\Delta m^2_{new}|$ and $\sin^2(2\theta_{new})$ (1 d.o.f.) lead to the constraints, $|\Delta m^2_{new}| > 1.5$ eV² (95%) and $\sin^2(2\theta_{new}) = 0.17 \pm 0.08$ (95%). The best fit value is at $|\Delta m^2_{new}| = 2.35 \pm 0.1$ eV² (68%) and $\sin^2(2\theta_{new}) = 0.165 \pm 0.04$ (68%).

The expected sensitivity for the presently proposed experiment is also shown in Figure 4 as a comparison. The integrated intensity correspond to (a) 2.5 x $10^{10}$ POT (protons on target) for the original beam intensity of about 30 kWatt of the previous CERN/PS experiments, (b) to 7.5 x $10^{10}$ POT for the newly planned 100 kWatt neutrino beam at CERN/PS and (c) and (c) to an hypothetical 300 kWatt neutrino beam.

*1.7 A more direct, new approach to neutrino oscillations.*

In all previously discussed experiments the time-dependence of a potential neutrino related oscillation pattern is not measured directly, the effect being observed *indirectly* at a *single* distance from the proton target, due to a resulting difference between the experimental data and the standard prediction of two neutrino.

However the direct measurement of a $\sin^2(2\theta_{new})$ oscillation pattern requires necessarily the (simultaneous) observation at different distances. It is only in this way that the values of $\Delta m^2$ and of $sin^2(2\theta)$ can be separately identified. The present proposal at the CERN-PS — combining the idea of the previous but never realized I216/P311-CERN experiment [15] with the hereby addition of the LAr TPC [11]— introduces therefore important new features, which should allow a definitive clarification of the LSND anomaly.

---

[1] Reactor experiment rates only

[2] According to neutrino analysis of Ref. [8].

The present proposal at the CERN-PS is based on the search for spectral differences of electron like specific signatures *in two identical detectors but at two different neutrino distances*, at the "Far" and the "Near" locations, respectively at 850 m and 127 m away from the source [12].

It is a very fortunate circumstance that in the case of the CERN-PS the $\nu_e$ spectra, expected at the level of 0.5 *% are very closely identical in the "Near" and "Far" positions* (Figure 5). The physical reason of this effect has to be identified in the fact that while the $\nu_\mu$ spectrum is dominated by the two body $\pi \rightarrow \mu – \nu_\mu$ decays, where the neutrino directions are narrowly distributed along the axis, the $\nu_e$ contamination is dominated by the three body decays of K and $\mu$ where there is a much wider the neutrino angular spread. This very relevant property of the beam has been verified measuring experimentally the radial distributions of $\nu_\mu$ and $\nu_e$ neutrino events.

This similarity is further enhanced by the fact that the "Near" and "Far" detectors have been designed with identical internal volumic dimensions and configurations.

In absence of oscillations, after some beam related small spatial corrections, the two energy spectra should be a precise copy of each other, independently of the specific experimental event signatures and without any need of Monte Carlo comparisons. Therefore an exact, observed proportionality between the two $\nu_e$ spectra implies directly the absence of neutrino oscillations over the measured interval of L/E: any resulting $\nu_e$ difference between the two locations, if observed, must be inevitably attributed to the time evolution of the neutrino species.

A key issue of the proposed experiment will be the detection capability of the genuine $\nu_e$ events and the very high level of rejection of the associated background events, in primis from the $\pi^0$ decay. As described in more detail further on, the LAr - TPC detector appears very well suited for this purpose, because of its excellent imaging and calorimetric capabilities, which allow very efficient electron - $\pi^0$ separation, together with unambiguous electron identification.

According to the present proposal the ICARUS T600 detector will be moved from the LNGS laboratory into the "Far" position of the CERN-PS neutrino beam (Hall B-191) after the completion of the presently running CNGS2 experiment at the end of 2012. An additional "clone" of the LAr structure using the same design is will be constructed for the "Near" configuration.

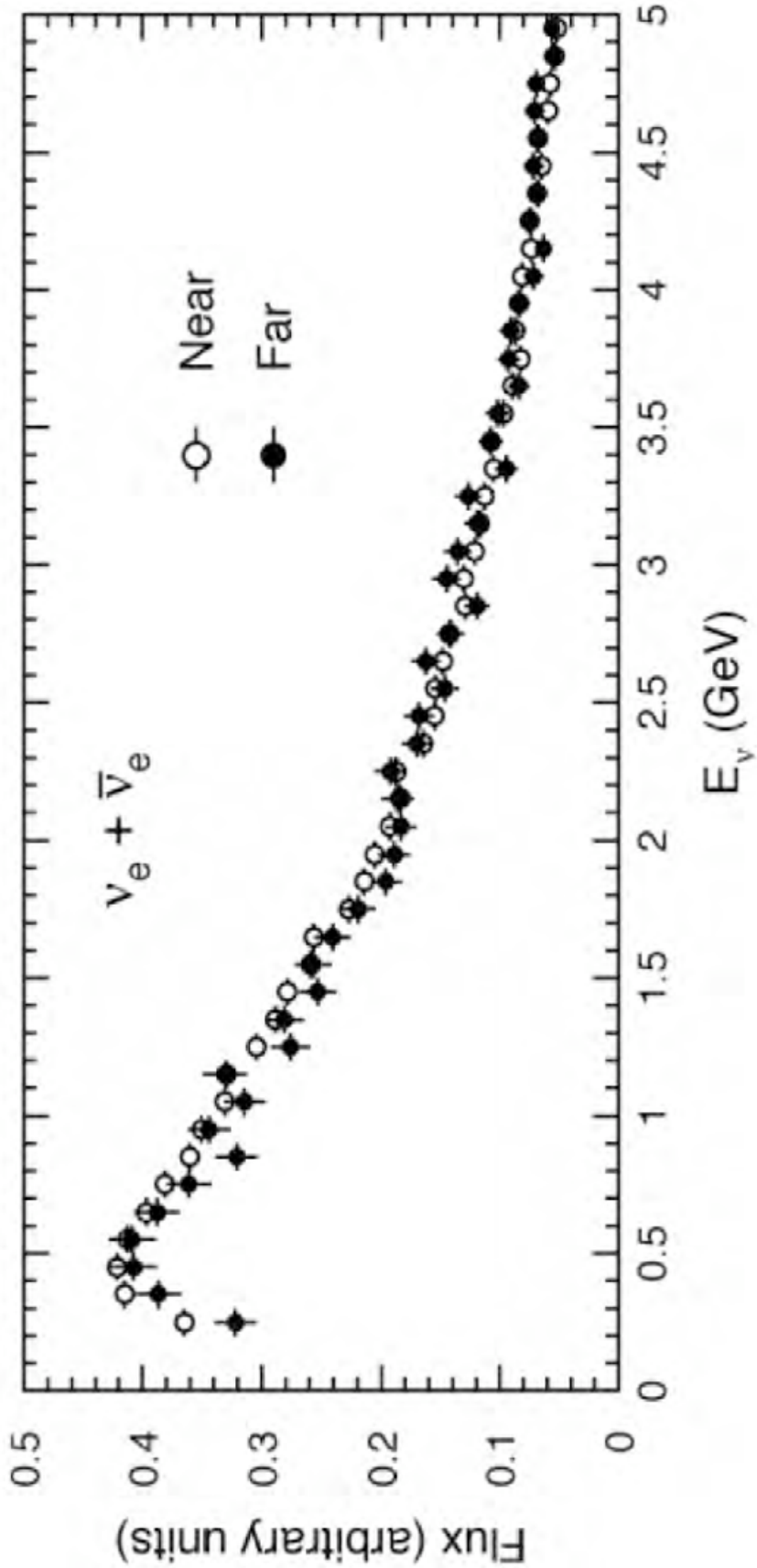


**Figure 5**.- The $\nu_e$ spectra [15], expected at the level of 0.5 % are very closely identical in the "Near" and "Far" positions of the CERN-PS. This specific property of the electron neutrino is due to the fact that they are produced exclusively by the K-decays which have a much wider angular distribution. The effect is enhanced by the fact that both detectors have been designed with identical experimental configurations.

*1.8 Other related experiments under consideration.*

To conclude, there are several different experiments that may hint at some important new phenomena in the neutrino sector (Figure 6). The disappearance results from an initial electron neutrino and the additional $\nu_\mu \rightarrow \nu_e$ oscillations are of course entirely different potential phenomena. However they may share the possibility of a common $\Delta m^2_{new}$ in the region of > 1eV$^2$. If confirmed without any doubt such a large mass difference will have an important role in the explanation of the existence of the Dark Mass in the Universe. The presence of the two alternate phenomena with different values of $\sin^2(2\theta_{new})$, if confirmed, will hint at the presence of an appropriate fourth neutrino mass matrix $U_{4,k}$ with k = $\mu$ and e.

The remarkable results of the previous considerations encourage further more elaborated experiments to finally determine the possibility of a neutrino anomaly beyond the Standard Model with the direct observation of the necessary oscillatory behaviour. *As stressed in Ref. [3] such a clearer experimental proof of the presence of the fourth neutrino becomes mandatory.*

Our presently proposed experiment should achieve these goals exploiting the very high selectivity for $\nu_e$ in the LAr –TPC at the optimal energy of a few GeV and the very close identity of the $\nu_e$ beams in the "Near" and "Far" positions. Both the disappearance rate and the MiniBooNE/LNSD electron anomalies can be searched with both the neutrino and antineutrino beams and with the $\nu_\mu$ and $\nu_e$ components of each of the beams. The very high counting rates and the chosen locations of the two detectors are optimal for the sensitivity required by such anomalies. The possibility of some hypothetical CPT violating effect can also be accurately probed.

Other complementary alternatives are being considered elsewhere and they are here briefly discussed. A new, dual Gallium experiment to search for sterile neutrinos at $\left|\Delta m^2_{new}\right| > 1$ eV has been described [16]. It consists in a very intense source of $^{51}$Cr at the centre of a 50–tonne target of Gallium metal, divided into two concentric spherical zones, whereby the neutrino capture rate is compared.

The direct test of a disappearance pattern for a sterile neutrino hypothesis has lead to the suggestion [17] [3] of the possible deployment at the centre of the ultra-low background detectors, such as Borexino, KamLAND and SNO+ of a ≈5 MegaCurie source of $^{51}$Cr or $^{37}$Ar, which produce narrow lines of electron *neutrinos*. In these detectors the leading process is the $\nu + e \rightarrow \nu + e$ elastic process on electrons, since the inverse β-decay process can only be detected at these energies by antineutrino on neutrons. Both sources produce also about 3 x 10$^{-4}$ internal bremsstrahlung γ-rays in the 200-600 keV range (1500 Curies), which must be strongly shielded in order to

permit the clean emergence in the detector of direct, on-line scintillation Compton-like signal due to neutrino interactions with the source.

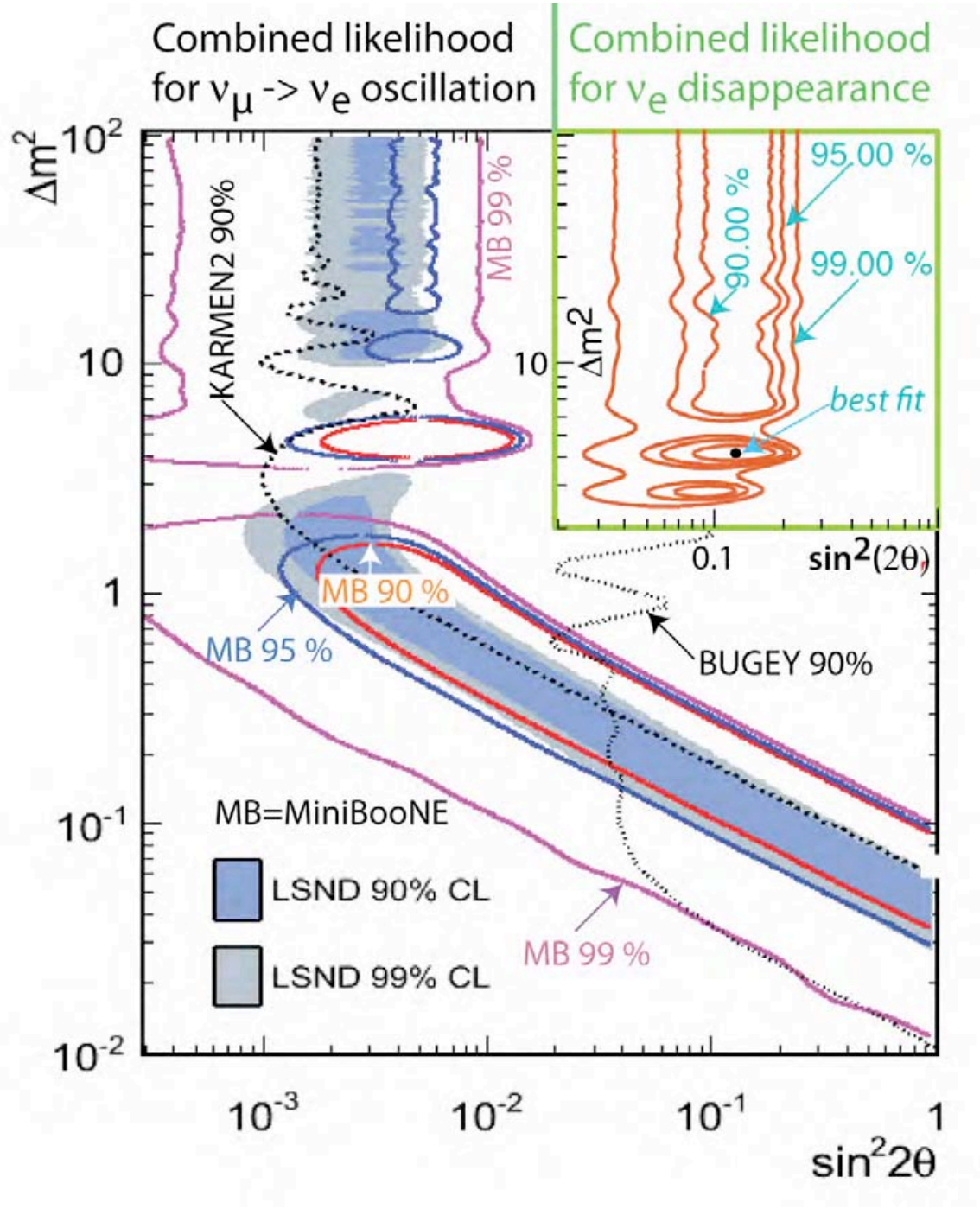


**Figure 6.-**Allowed regions in the $|\sin^2_{new}| - |\Delta m^2_{new}|$ plane for the LSND /MiniBooNE antineutrino anomaly and for the combined results from Ref. [3] for the electron antineutrino anomaly in the disappearance rate. While the values of $\Delta m^2_{new}$ may indeed have a common origin, the difference of the values of $\sin^2(2\theta_{new})$ may reflect in the four neutrino hypothesis the structure of the $U_{4,k}$ mass matrix with k = $\mu$ and e.

Such a Compton-like $^{51}$Cr induced ν process is also contaminated with a comparable signal due to solar neutrinos and of various backgrounds coming from radio contaminants, subtracted statistically with a source-in source-out procedure. The $^{51}$Cr source produces neutrinos with the reaction $^{51}Cr + e^- \rightarrow {}^{51}V + \nu_e$ and a half-life of 27.7 days with four energy lines: 0.751 MeV (9%), 0.746 MeV (81%), 0.431 MeV (1%), 0.426 MeV (9%). Assuming for instance $\left|\Delta m^2_{new}\right| = 2.0\ eV^2$, the first minimum of R at $E_{ve} \approx 0.750\ MeV$ occurs after the rather short distance of L = 46 cm.

In Ref. [17] the alternative of *antineutrino* production by a 36 kg pure $^{90}Sr/^{90}Y$ source and 5 MegaCurie (1.75 x $10^{17}$ c/s, ≈40 kWatt) has been considered. The source generates $\bar{\nu}_e$ as $^{90}Sr \rightarrow {}^{90}Y + \bar{\nu}_e + e^-$ ($\tau_{1/2} \approx 28.5y$) followed by $^{90}Y \rightarrow {}^{90}Zr + \bar{\nu}_e + e^-$ ($\tau_{1/2} \approx 64.8h$), with the end point of 2.27 MeV for the daughter $^{90}$Y. The $^{90}$Y reaction has sufficiently high energy to observe the inverse β-decay process on protons, $\bar{\nu}_e + p \rightarrow e^+ + n$ with an energy threshold of 1.8 MeV. The inverse β-decay process will be much cleaner if the detection of the delayed neutron is also exploited, the remaining signals being primarily the ones due to distant Reactors and of Earth's geo-$\bar{\nu}_e$ from Th/U.

In Ref. [17] it has been assumed that the source will be at 8.25 m from the centre of the spherical 100 ton fiducial volume of the BOREXINO detector. The event rate is reasonable, about 3 ev/hour, but the direct oscillatory effect may be significantly washed out since — for instance at $\left|\Delta m^2_{new}\right| = 2.0\ eV^2$ — the first minimum of R occurs at the rather short distance of L = 1.2 m. Presumably a smaller dedicated detector with a much more compact geometry could enhance the presence of the oscillatory signal. The main expectations of Ref. [17] are shown in Table 2.

[a] ***Table 2***. *Time of exposures, expected backgrounds, signals according to Ref. [17]*

| ***Experiment*** | ***Reaction*** | ***Time (days)*** | ***Background*** | ***Signal*** |
|---|---|---|---|---|
| $^{51}$Cr | $\nu_e - e$ scattering | 60 | 4380 | 4006 |
| $^{90}$Sr | $\bar{\nu}_e - e$ scattering | 180 | 17460 | 25971 |
| $^{90}$Y ($^{90}$Sr) | Inverse β-decay | 180 | ≈ 5 | 13278 |

In Ref. [18] more elaborate and intense Reactors have been also discussed, which may permit to come at a sufficiently close distance from the core in order to improve the ILL results with the direct observation of the oscillatory behaviour.

Other experiments plan to search directly for the $\bar{\nu}_\mu \rightarrow \bar{\nu}_e$ anomaly with high energy proton accelerators. The beginning of the operation of the MicroBooNE experiment [19] is foreseen by the end of 2013 from the 8 GeV Booster at FNAL. Like the presently proposed experiment MicroBooNE at FNAL is a detector based on the LAr TPC technology. However the present proposal, MicroBooNE has a) only 60 ton of fiducial mass; b) a single detec-

tor and therefore heavy reliance on Montecarlo calculations and experimental biases; and c) a much smaller $\bar{\nu}_\mu$ flux and cross-sections[3].

The huge reduction factor makes the determination of the expected anomalies *with antineutrino* at MicroBooNE rather difficult.

The new experiment OscSNS [20] has been proposed at ORNL with pions at rest, but with a higher intensity spallation source (1.4 MW). The detection principle is identical to the one of LSND. The new detector has essentially the same mass (800 t) as the one already used at LAMPF, but with higher PMT coverage and at a distance of ~ 60 m from the SNS beam stop at ORNL. If approved, the experiment might begin to operate around 2013 with an appearance signal and about three times the statistics of LNSD for the nominal SNS intensity.

[3] In the case of Argon, the reduction factor is much more significant than the one relative to the liquid scintillator of MiniBooNE, about $1/0.08 = 12$ for energies < 430 MeV and about 7.1 at 1000 MeV. At low energies, anti-neutrino interactions on nuclei are disfavoured because of the low momentum transfer that enhances the Pauli blocking effect. Also the isotopic composition, with an excess of neutrons, is unfavourable to anti-neutrinos. As a consequence, the ratio of neutrino to antineutrino cross sections on nuclei increases steadily at low energies.

# 2 The development and the operation of the LAr TPC.

*2.1 Principle of operation.*

Bubble chambers have had a major role in neutrino physics: for instance the well known Gargamelle bubble chamber, in spite of its relative small sensitive mass compared to other electronic calorimetric detectors has contributed in an essential way to the discovery of Neutral Currents and of the Electro Weak components of the Standard Model.

These future detectors however should require additional features: they should not involve pressurized liquids, they must be continuously sensitive rather than pulsed, they must obey to the strict safety requirements of underground laboratories and they must be capable of reaching a sensitive mass ultimately of many tens of thousands of tons (as a comparison the Gargamelle chamber had a sensitive mass of 3.14 tons of freon).

No doubt in the future the use of a totally sensitive imaging detector may have an unique role not only in neutrino physics, but also in proton decay and the search for WIMP like events coming from dark matter.

The LAr-TPC technology, first proposed by Carlo Rubbia in 1977 [11], has been developed by the ICARUS group since about two decades [21]. The "bubble chamber like" observation of the neutrino events permits to identify precisely the features of individual events [22]. This is an important difference with respect to all previously reported observations which have been based on the necessarily more primitive observation of Cerenkov rings produced by PM's at the surface of the detector volume and which are mostly limited to quasi-elastic events.

The technology of the LAr-TPC [23] is conceived as a tool for a completely uniform imaging with high accuracy of massive volumes. The new method of imaging in a noble liquid is based on a truly novel concept of free electron drift as a function of the time, in order to observe the true "image" of the track with an accuracy of the order of 1 $mm^3$, thus extending to a liquid the idea of the TPC already described for a gas, originally proposed by G. Charpak et al. [24]. The passage from a gas to a liquid is not entirely trivial, since the density is about a factor 1000 larger and therefore a corresponding much higher purity is necessary. The length of the drift of electrons in ultra-pure noble liquid becomes an asset and it must be made as long as possible, up to meters, corresponding to equivalent Oxygen contents of the order of a few tens of ppt (parts per trillion).

The method has been extensively studied by our group over two decades with liquid Xenon (LXe) and Argon (LAr), with and without significant amounts of liquid methane in order to enhance the presence of free electrons,

firstly with small laboratory-like detectors and later with much larger detectors developed with the help of industry.

The operational principle of the LAr-TPC is based on the fact that in highly purified LAr ionization tracks can be transported practically undistorted by a uniform electric field over macroscopic distances. Imaging is provided by a suitable set of electrodes (wires) placed at the end of the drift path continuously sensing and recording the signals induced by the drifting electrons. Non-destructive read-out of ionization electrons by charge induction allows detecting the entire signal of electrons crossing subsequent wire planes with different orientation. This provides simultaneously several projective views of the same event, hence allowing space point reconstruction and precise calorimetric measurement.

**Table 3.** Some relevant parameters for LAr and heavy Freon bubble chamber

| Material | Argon | Freon | |
|---|---|---|---|
| Z/A | 0.45 | 0.46 | |
| Volumic concentration of air | 0.934 | – | % |
| Main isotope | 99.6 ($^{40}$Ar) | ($CF_3Br$) | % |
| Melting point @ 1 atm | 83.8 | – | K |
| Boiling point @ 1 atm. | 87.3 | 320. | K |
| Latent heat capacitance | 1.078 | – | kJ/kg/K |
| Density @ boiling point | 1.4 | 1.5 | g/cm$^3$ |
| dE/dx for m.i.p. | 2.12 | 2.27 | MeV/cm |
| Critical energy for electrons | 31.7 | 27.6 | MeV |
| Electron-ion pair energy | 23.6 | – | eV |
| Radiation length | 14.0 | 11. | cm |
| Moliere radius | 9.3 | 8.5 | cm |
| Interaction length | 83.6 | 78.3 | cm |
| Electron mobility | 500. | - | cm$^2$ V$^{-1}$ s$^{-1}$ |
| Electron drift velocity @0.5 kV/cm | 1.56 | | mm/$\mu$s |
| Ion drift velocity @0.5 kV/cm | ≈ 1. | | cm/s |
| Electron diffusion coefficient | 4.8 | - | cm$^2$ s$^{-1}$ |
| R.m.s. «bubble» size @ 0.5 kV/cm | | | |
| (1) After 1 m drift | 0.6 | 1.3 | mm |
| (2) After 5 m drift | 1.3 | 1.3 | mm |
| Ionization electron @0.5 kV/cm | ~2.5 x10$^4$ | – | e$^-$/MeV |
| Scintillation photon prod. energy | 19.5 | – | eV |
| Scintillation (zero E field) @ 128 nm | ~5 x 10$^4$ | – | ph/MeV |
| Refractive index @ visible light | 1.24 | – | |
| Break-down voltage | ~1.1 x 10$^6$ | – | V/cm |

Liquid Argon, with its 0.9 % of air, is the only noble gas, which has today a vast industrial utilization, since it can be easily produced in very large quantities and with a remarkably low cost. Its main production is as part of the liquefaction of dry air and it can be easily separated by fractional distillation for instance from Nitrogen and Oxygen. Some of the main parameters relative to its use as a LAr-TPC are given in Table 3. These main parameters, like the density, dE/dx, radiation and interaction lengths, are rather close to the ones of the above mentioned Gargamelle bubble chamber. However the high resolution of the nuclear and electromagnetic cascades can now provide an accurate determination of the events. Multiple scattering along the very many points of a relativistic muon track can be used to measure the muon momentum. Stopping particles are recognized by the length of the track and dE/dx variation along the end part of the path. Therefore, contrary to the case of a bubble chamber, the accurate determinations of the above parameters permit to arrive to a rather complete reconstruction of the events also in absence of a magnetic field. On the other hand a magnetic field with a huge volume as required by the present (T600) and especially the future dimensions of even larger LAr chambers would imply an astronomical magnetic energy.

The key features for the success of the LAr–TPC technology are therefore new industrial purification methods at an exceptional level, especially of the remnants of Oxygen and Nitrogen, which have to be initially and continuously purified. Indeed the longest drift distance at which one can operate is inversely proportional to the residual contamination due to several electro-negative gases. Although several polar chemicals may be present in the volume, we have used the concept of Oxygen equivalent contamination. The best result, reported within the ICARUS Collaboration in a smaller 120 litres detector is a mean electron lifetime in excess of 15.8 ms at 90 % C.L. at a standard electric field of 500 V/cm, corresponding to ≈ 20 ppt (part per trillion), namely a ≈ 2.0 x $10^{-11}$ molecular content with respect to Argon [25]. The short path length used in this measurement (30 cm) has been compensated by the high accuracy in the observation of the specific ionization of cosmic rays muons at sea level (LNL, Legnaro, Italy). At this field the electron speed is approximately of 1.5 mm/$\mu$s: the measured lower limit to the experimental free electron lifetime $\tau$ corresponds to an attenuation of about 15 % for a longest drift of 5 meters and 500 V/cm, opening the way to exceptionally long drift distances, as proposed for instance by the MODULAr programme [26].

**Figure 7**. The ICARUS T600 detector installed in Hall B at LNGS.

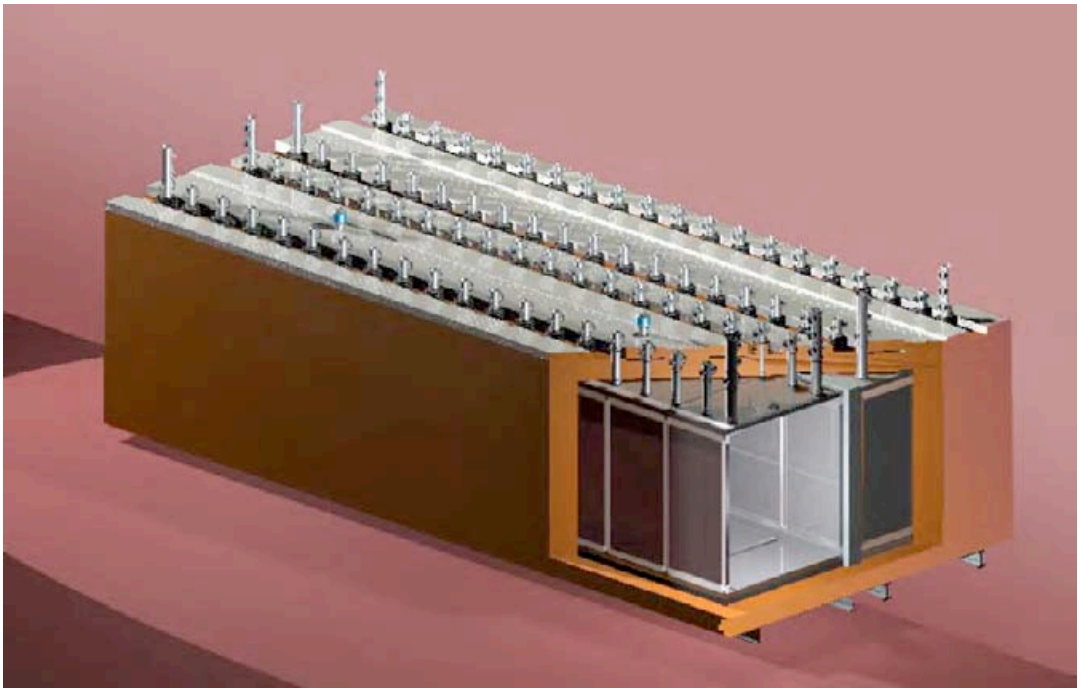

**Figure 8.** The ICARUS T600 detector schematics, showing both semi-modules and the common insulation surrounding the detector. Inner structures and feed-through's are also shown.

## *2.2 The ICARUS 600 ton LAr detector.*

The ICARUS T600 detector [27] presently in operation underground in Hall B of LNGS in a neutrino beam from the CERN-SPS, is the largest liquid Argon TPC ever built, with a size of about 600 t of imaging mass (Figure 7). The design and assembly of the detector relied on industrial support and represents the application of concepts matured in laboratory tests to the kton-scale.

### *2.2.1 General description of the T600.*

The ICARUS T600 LAr detector consists of a large cryostat split into two identical, adjacent half-modules, each filled with about 380 t of ultrapure liquid Argon (see Figure 8). Each half-module houses two Time Projection Chambers (TPC) separated by a common cathode, a field shaping system, monitors and probes, and two arrays of photo-multipliers. Externally the cryostat is surrounded by a set of thermal insulation layers. The detector layout is completed by a cryogenic plant made of a liquid Nitrogen cooling circuit, maintaining the LAr temperature uniform, and by a system of LAr purifiers. Each TPC is made of three parallel planes of wires, 3 mm apart, facing the drift region, with wires oriented at 0° and ± 60° from the horizontal direction. By appropriate voltage biasing, the first two planes (induction planes) provide signals in non-destructive way, whereas the charge is finally collected in the last one (collection plane). The maximum drift path, i.e. the distance between the cathode and the wire planes, is 1.5 m and the nominal drift field 500 V/cm. The total number of wires in the T600 detector is about 53000. The signals coming from each wire are independently digitized every 400 ns. The electronics was designed to allow continuous read-out, digitization and independent waveform recording of signals from each of the wires of the TPC. The measurement of the time of the ionizing event, the "$T_o$ time" which can be determined via the prompt scintillation light produced by ionizing particles in LAr, together with the knowledge of the electron drift velocity, provides the absolute time and hence the position of the tracks along the drift coordinate.

### *2.2.2 Technical description.*

In the following an in-depth description of the detector details will be given, with the help the technical drawings shown in Figure 9. Numbering in the Figures and referred in the text corresponds to the items listed in Table 4. For additional details we refer to Ref. [27] related to the operation of the first half-module T300 in Pavia.

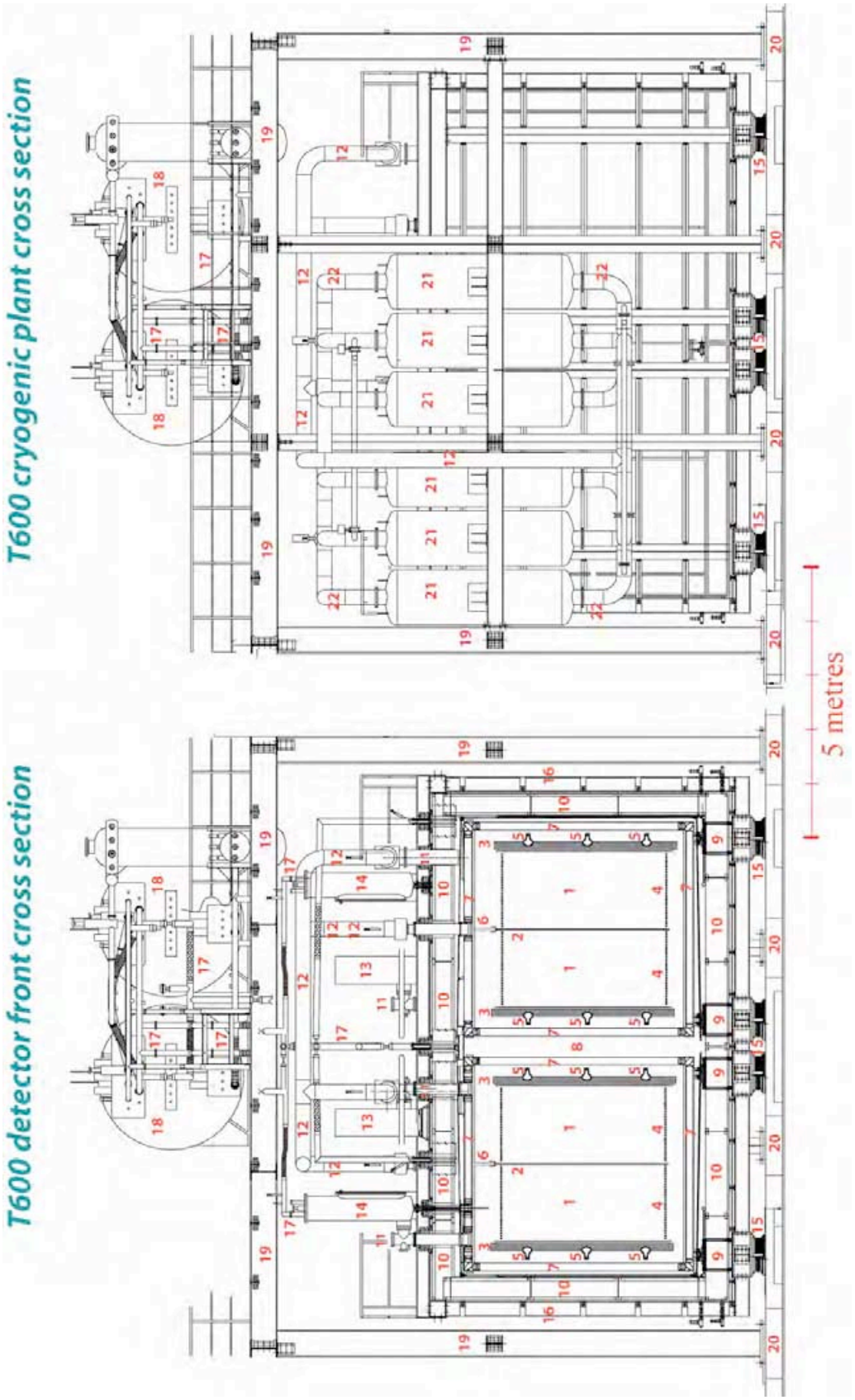


**Figure 9.** Technical drawings of the T600 detector and cryogenic equipments, as realized at LNGS Hall-B. Numbered items are explained in the text.

The ICARUS T600 LAr detector consists of a large cryostat split into two identical, adjacent half-modules, with internal dimensions $3.6 \times 3.9 \times 19.6$ m$^3$ each (**1**).

Each half-module houses two Time Projection Chambers (TPC) (**4**) separated by a common cathode (**2**), a field shaping system (**3**), monitors and probes, and two arrays of photo-multipliers (**5**), coated with TPB wave-shifter. Externally the cryostat is surrounded by a thermal insulation layer. The two half-modules are not cryogenically independent, being the thermal insulation and the Nitrogen cooling system in common for the whole detector (**10** and **17**).

**Table 4**. Legend of the T600 LAr-TPC detector. Numbers refer to Figures 9 and 17.

| Item | Description |
|---|---|
| 1 | Drift ultra-pure LAr Volume (300 ton) |
| 2 | HV cathode (150 kV) |
| 3 | Wire chamber readout planes (3) |
| 4 | Drift field shaping rings |
| 5 | Light collecting PM's |
| 6 | HV feed through (150 kV) |
| 7 | Aluminium Honeycomb container box |
| 8 | Evacuated volume (cold) |
| 9 | Supporting and insulating feet |
| 10 | Thermal insulation and containment |
| 11 | Chimneys for readout electronics |
| 12 | Evacuation piping |
| 13 | Racks for electronic readout |
| 14 | Gas recirculation & purification |
| 15 | Supporting feet |
| 16 | Protective gridding |
| 17 | Nitrogen cooling circuits |
| 18 | Liquid Nitrogen storage |
| 19 | External supporting structure |
| 20 | Main basement |
| 21 | Nitrogen re-liquefaction system |
| 22 | Cryogenic plant |
| 23 | Liquid transfer pump |
| 24 | Oxysorb/Hydrosorb filter in liquid phase |

The outer dimensions 4.2 x 3.9 x 19.9 m$^3$ of each LAr container (**7**) were defined by the requirement that the LAr container (cold vessel) had to be transported through highways into the underground Gran Sasso Laboratory and installed there.

The basic elements of the cold vessels are panels with a thickness of 150 mm and a surface of 2.0 x 3.9 m$^2$ in the case of side walls and a surface of 2.0 x 3.6 m$^2$ in the case of top and bottom walls. They are made of aluminium honeycomb, surrounded by frames of aluminium profiles and sandwiched

between two aluminium skins. The panels are welded together to form a parallelepiped box ("T300" half-module). The two end caps (3.6 x 3.9 $m^2$) both formed by two special panels joined by an H-shaped profile, are added at the end.

Holes and chimneys (**11**) for the way out of signal cables of the internal detectors and control instrumentation are located on the ceiling of the container, in correspondence with the two frames of the wire chambers. The ports (**14**) for LAr filling, gaseous Argon (GAr) recirculation and other services like vacuum instrumentation and safety disks, as well as two flanges (manholes) of 500 mm diameter used for inspection and for the final assembly operations, are also located on the top side.

The two sub-modules are surrounded by a common thermal insulation layer (**10**), which is realised by evacuated Nomex™ honeycomb panels (0.4 m thick) to form a closed vacuum-tight box, with nominal heat losses of about 10 $W/m^2$.

A thermal shield is used, circulating boiling Nitrogen ($N_2$) (**17**), to cool down the apparatus and to compensate the heat losses through the thermal insulation box, in order to maintain uniform and stable the cryostat bulk temperature. Cooling of the cryostat is performed by circulating 2-phase $N_2$ at 84 K. The circulation speed is defined by the request to maintain a thermal uniformity within 1 °C in the LAr bulk. The LAr cryostat is operating at a slight overpressure of 100 mbar at a temperature of about 89 K.

The cryostat is filled with ultra-pure Argon obtained starting with commercial liquid (with a typical content of $H_2O$, $O_2$, $N_2$ of the order 1 ppm) filtered at the cryostat input by means of commercial filters. To ensure an acceptable initial LAr purity, the detector is evacuated (**12**) to a pressure of the order of $10^{-4}$ – $10^{-5}$ mbar, before filling, in order to perform an appropriate out-gassing of the cryostat internal walls and all the detector materials.

Moreover, each half-module is equipped with two gas (**14**) and one liquid recirculation systems (**23** and **24**), both required to attain a very high free-electron lifetime (several ms) in less than one month. The continuously active gas recirculation units (≈ 25 GAr $Nm^3/h$ each at maximum rate) collect the gas from the chimneys that host the cables for the wire chamber read-out. The gas is re-condensed into a $LN_2$ re-condenser with the liquid dropping into an Oxysorb/Hydrosorb filter placed below the re-condenser. The purified Argon is sent back into the LAr container just below the LAr surface.

The main purpose of the liquid recirculation (circulating ~ 2 $m^3/h$, corresponding to a full recirculation in about 6 days) is to purify the Argon just after filling and until the required LAr purity is reached. In addition, it has to restore the purity in case of accidental pollution during the detector run, e.g. due to a sudden depressurization of the gas volume. Liquid recircu-

lation units consist of an immersed, cryogenic, liquid transfer pump (**23**) placed inside an independent dewar. The circulated LAr goes through standard Oxysorb/Hydrosorb filter (**24**) before being re-injected into the cryostats.

The cold power request for the ICARUS T600 module is summarized as follows: (1) insulation losses (comprehensive of heat input through joints, cryostat feet and cables) plus Nitrogen cooling (circulation pumps and distribution lines); (2) GAr re-circulation and purification systems (4 systems for the full T600); (3) LAr re-circulation and purification systems (2 systems/T600). The whole Nitrogen re-liquefaction system (**21**) is composed of 10 cryo-cooler units (about 4 kW of cold power each) in order to cover up to 40 kW of global cold power, guaranteeing to abundantly cover the basic consumption of the detector. Each unit can be switched on/off independently to deliver the actual cold power needed by the system.

Two $LN_2$ liquid storage tanks (**14**) are installed (30 $m^3$ each) on the top level of the T600 service structure and used as "buffer" for the cryo-coolers. One of the two tanks is used as LAr storage tank during the initial T600 filling phase. During stable operation, both tanks are used for Nitrogen storage in order to guarantee a higher Nitrogen reservoir in case of need.

Each of the two LAr cryostats hosts the different internal detector subsystems and the control instrumentation, namely the two TPC chambers (**3**) positioned on the opposite, vertical long sides of cryostat and the relative HV electrode system, a central cathode (**2**) and field shaping electrodes (**4**), for the read out of the ionization charge, the PMT system (**5**) for the scintillation light detection, sensors and probes of the slow control system. The distance of the two TPC's is 3.00 m with the cathode placed in the middle, for a maximum drift path of 1.5 m.

The cathode (**2**) is realized by an array of nine panels of punched stainless-steel sheets. The drift electric field is generated by biasing the central cathode at a negative HV referred to the potential of the first wire plane; the nominal 500 V/cm drift field requires 75 kV on the cathode, provided by a specially designed ultra-high vacuum cryogenic feed-through tested at more that 150 kV (**6**). The electric field in each drift volume is kept uniform by means of the field shaping electrodes (**4**), i.e. 29 rectangular rings for each wire chamber which are set at a potential linearly decreasing from the cathode to the first wire plane. Hence it guarantees a constant drift velocity inside the drift volumes. The biasing potentials of the race tracks are obtained through resistive voltage degraders, in steps of 25 MOhm each. The current flowing in each degrader ranges from 100 to 200 $\mu$A for HVs ranging from 75 to 150 kV.

Each TPC (**3**) consists of a system of three vertical parallel planes of wires (17.95 x 3.16 $m^2$ of surface) 3 mm apart from each other. The first faces the drift region, with horizontal wires, the other two have the wires at ± 60° from the horizontal direction. By appropriate voltage biasing, the first two planes (induction planes) provide signals in non-destructive way, whereas the charge is finally collected in the last one (collection plane).

TPC wires are made of AISI 304V stainless-steel with a wire diameter of 150 μm: the length of the wires ranges from 9.42 to 0.49 m depending on the TPC plane type and on the actual position of the wire in the plane itself. The wire-frame design is based on an innovative concept already used in T600: the variable geometry design (weight bridge). The beams of the wire frame are, in fact, movable. The upper and the lower horizontal beams are rigidly connected to each other on the back side of the frame by a set of calibrated springs, while the vertical beams are connected to the sustaining structure also by springs. This allows: (1) to set the tension of the wires after easy installation, (2) to compensate for possible overstress during the cooling and LAr filling phases and (3) to counteract the flexibility of the structure. This design was successfully adopted in ICARUS T600 for more that 53000 wires, none of which broke during testing in Pavia, the moving of the detector to LNGS and the operation at LNGS.

A set of 8 inch ETL-9357-FLA™ photomultipliers (**5**) coated with TPB wave-shifter are installed internally the cryostats, 20 PMTs in the first half-module and 54 in the second one, behind the wire chambers to detect the prompt scintillation light for triggering and T = 0 timing purposes.

Once the cryostat is filled, the structure is totally immersed in LAr. The stainless-steel chimneys (**11**), aligned in two rows on the aluminium ceiling of each T300 cryostat (20 per row) and terminated with special vacuum-tight feed-through flanges (INFN patent RM2006A000406), allows the passage of the wire signal cables (572 per flange) and that of other detector subsystem (PMT's) and control instrumentation. Each flange is connected to a single electronic rack (**13**) where the front-end electronic, the digitisers and the memory buffers are hosted for the readout of 572 channels.

The ICARUS-T600 read-out architecture is based on an analogue chain consisting of a front-end low noise charge sensitive pre-amplifier, based on a custom designed BiCMOS dual channel IC with a j-FET input stage, followed by a baseline restorer to reduce low frequency noise. The gain of the front-end amplifier and filter is 1 V / 164 fC. The amplifier noise is ~ 1200 electrons at detector capacitance of 450 pF (signal wire plus cables).

The signals coming from each wire are independently digitized every 400 ns by a 10 bit FADC. This scheme is implemented on a single VME-like analogue board (CAEN V789) hosting 32 channels amplifiers, multiplexers,

ADC's and a 20-bit, 40 MHz serial link that sends the data to a digital board (CAEN V791) for the buffering of events.

The electronics is designed to allow continuous read-out, digitization and independent waveform recording of signals from each wire of the TPC. The measurement of the time of the ionizing event, the "T=0 time" which can be determined via the prompt scintillation light produced by ionizing particles in LAr, together with the knowledge of the electron drift velocity provide the absolute position of the tracks along the drift coordinate. It is satisfactorily used in the ICARUS-T600 run at LNGS.

The T600 experimental set-up at LNGS has been realized inserting the two T300 half-modules, transported from the Pavia INFN laboratory, into the insulation vessel (**10**), the supporting structure (**19**) and a protective containment vessel (**16**), which were built "in-situ". The insulation structure is mounted on a series of supporting feet (**20**) designed to fulfil strict seismic and insulation requirements. The full T600 plant installation has been completed with the integration of specific sub-systems including cryogenic plant (**22**), $N_2$ re-liquefiers (Stirling compressors **21**) and LAr re-circulators (**23**), LAr purifiers (**24**), read-out electronics and the DAQ system (**13**). Globally the set-up in Hall B at LNGS required a surface of about 12 x 37 $m^2$, and a height not exceeding 12 m.

*2.2.3 Early operation of T600 in LNGS.*

The T600 final commissioning at LNGS took place during the first months of 2010, leading to the successful filling with liquid Argon and the detections of the first CNGS neutrino events at the end of May 2010 (Figure 10).

Before filling the detector with ultra-pure liquid Argon the cryostats have been evacuated and kept under vacuum to reduce electronegative impurities and minimize the out-gassing from detector materials. Next, the cryostats were filled with ultra pure Argon gas at an over-pressure of 100 mbar and cooled down with 10 Stirling $LN_2$ liquefiers (cold power: 40 kW), circulating in the cold screens. Additional cooling power was available using liquid Nitrogen from a 30 cubic meter storage.

Ultra pure liquid Argon was injected at the rate of ~ 2 $m^3$/hour. Both modules were filled with a total amount of 610,511 litres delivered in 2 weeks. The Stirling $LN_2$ liquifiers operated continuously without problems. As discussed in the next paragraph, the progressive purification process in the liquid phase has been performed.

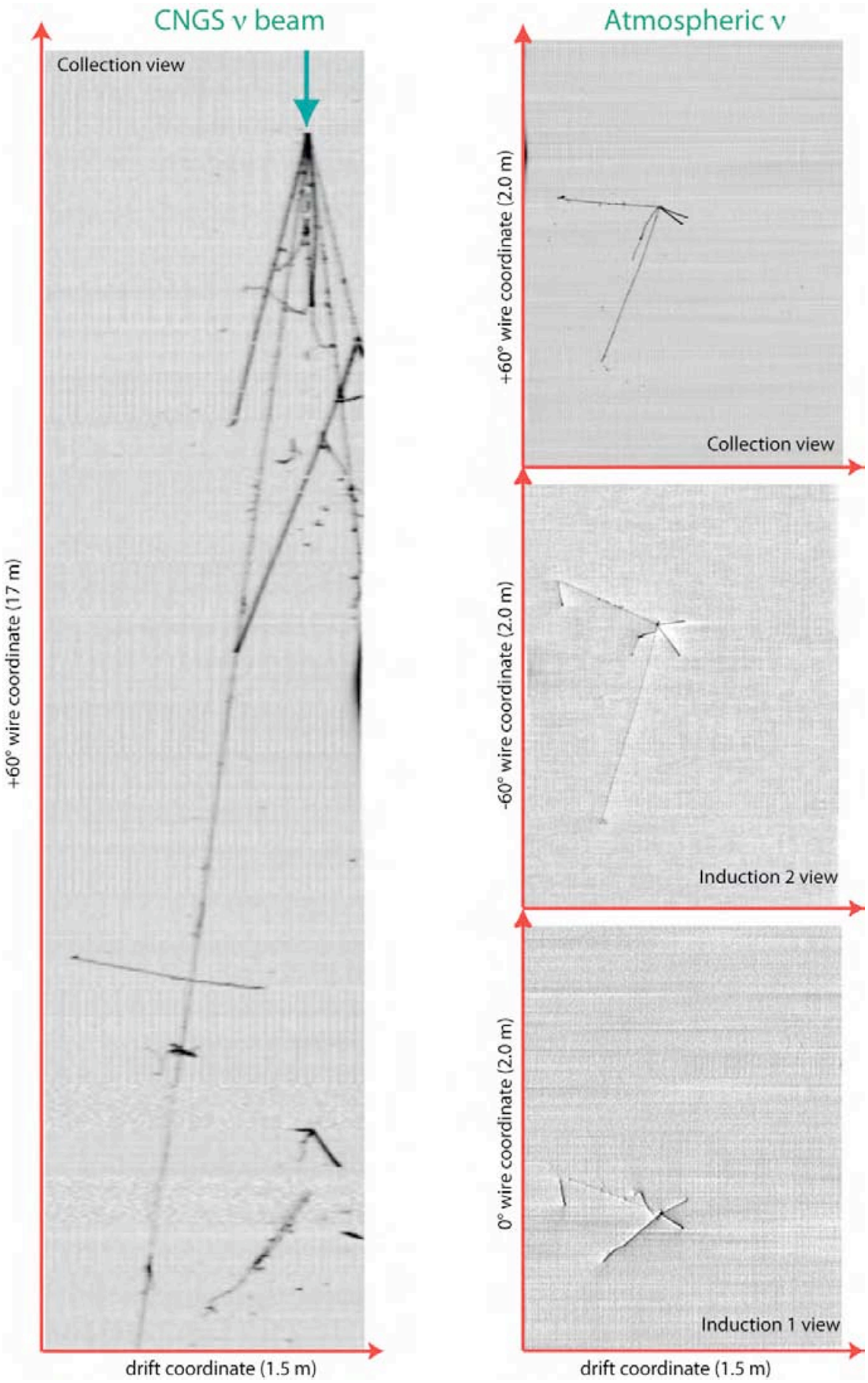


**Figure 10.** Left: high energy CC $\nu_\mu$ event from the CNGS beam recorded in the ICARUS T600 detector (collection view is shown). Right: multi-prong low energy atmospheric neutrino interaction recognized in all three view; total visible energy is 770 MeV including quenching and electron lifetime correction.

*2.2.4 Experimentally achieved LAr purity.*

The free electron lifetime $\tau_{ele}$ is a key element in the operation of the LAr-TPC. As already pointed out, the length of the drift of free electrons must be made as long as possible, up to meters, corresponding to equivalent Oxygen purities of the order of tens of ppt (parts per trillion).

The key features for the practical success of the LAr–TPC have been new industrial purification methods at an exceptional level, especially of the remnants of Oxygen and Nitrogen, which have to be initially and continuously purified. Indeed the longest drift distance at which one can operate is inversely proportional to the residual contamination due to several electronegative gases. Although several polar chemicals may be present in the volume, we have used for $\tau_{ele}$ the concept of Oxygen equivalent contamination ($\tau_{ele}[ms] \sim 0.3/N[ppb]$).

As already pointed out the best result [25] so far reported by our group has been with a smaller detector and the standard electric field of 500 V/cm and a free electron drift speed of approximately of 1.5 mm/μs, corresponding to ≈ 20 ppt (part per trillion), namely a ≈ 2.0 x $10^{-11}$ molecular content with respect to Argon. This represents an electron lifetime $\tau_{ele}$ in excess of $\tau_{ele} > 15.8$ ms at 90 % C.L. In view of the much larger volumes required and the complexity of the associated equipment, the free electron lifetime $\tau_{ele}$ as a function of the initial purification is expected to be at least initially somewhat smaller than what just reported in the small chamber prototype.

In 2001 the initial test in Pavia with a first T600 half-module (T300) has shown an increasing lifetime as a function of liquid purification time with a best result of 1.8 ms, but after as long as a three months of activity. Much progress in the recirculation technologies has permitted very considerable improvements with respect to this early result.

The measurements at LNGS have been performed with the help of tracks due to the vertical cosmic ray muons, naturally occurring at the approximate rate of 1 event/$m^2$/hour and measuring the electron attenuation as a function of the electron drift time.

The measurements at LNGS have been performed with the help of tracks due to the vertical cosmic ray muons, naturally occurring at the approximate rate of 1 event/$m^2$/hour and measuring the electron attenuation as a function of the electron drift time.

With the newly produced liquid purification process, after only 900 hours a stable and constantly growing value of the free electron lifetime of the order of $\tau_{ele} = 5\ ms$ has been observed experimentally for the T300 West cryostat in the Hall B of LNGS; the highest recorded value exceeds so far the *7 ms,* corresponding to a maximum charge attenuation of 13% for a full drift distance.

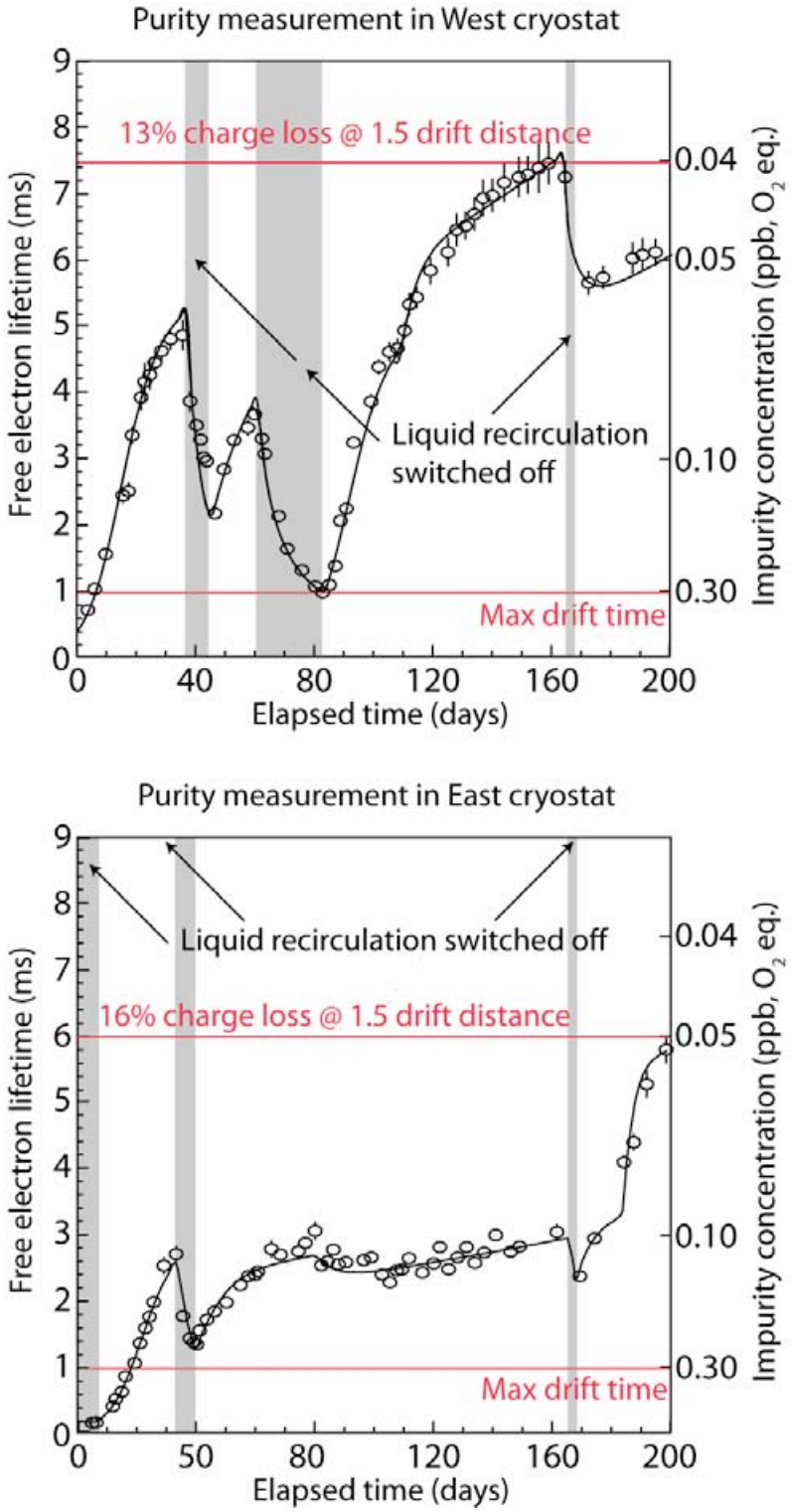


**Figure 11.** Free electron lifetime evolution in the West (top) and East (bottom) cryostats as a function of the elapsed time. For details see the text. The differences in the two distributions are due to the commissioning of the recirculating pumps which have experienced a number of interruptions and modifications.

In the East cryostat the best value of the free electron lifetime $\tau_{ele}$ is also exceeding *6 ms* after tuning and optimization of the recirculation system. The different behaviour of the impurities evolution in the two cryostats is under investigation. We remark that the initial impurity level of the East cryostat was about a factor 10 larger than the one of the other cryostat (N = 5.2 ppb and 0.6 ppb $O_2$ equivalent respectively). Figure 11 shows the time evolution of the free electron lifetime for the West and East cryostats.

Pumps maintenance required few stops of the LAr recirculation lasting several days, resulting in sudden degradation of the purity, which however never went below 1 ms.

The evolution of the residual impurity concentration can be described with a simple model as $dN(t)/dt = -N/\tau_R + k_L + k_D\, exp(-t/\tau_D)$ where $\tau_R$ is the time needed to recirculate a full detector volume, $k_L$ is the total impurity leak rate and $k_D$ is the internal residual degassing rate assumed to vanish with a time constant $\tau_D$. Uniform distribution of the impurities throughout the detector volume is also assumed, as experimentally supported by the lifetime measurement with muon tracks in different regions of the TPC's.

Fitting the data with this model yields a recirculation time of 5 days with one day fluctuation after each recirculation stop, in agreement with the nominal pump speed, and extremely low leak rates (< few ppt/day $O_2$ equivalent of impurity concentration) in the both half-modules. Internal initial degassing rate seems to be higher in the East module, resulting in a slightly worse purification rate.

The fit can be used also to determine the amount of impurities continuously generated inside the cryostats, respectively of 7.2 and 20 ppt/day (part per trillion, $O_2$ equiv.). This amounts to about 2.2 x $10^{-3}$ and 6.0 x $10^{-3}$ gram/day of Oxygen equivalent, polluting each of the two 300 ton LAr cryostats (a hair in a hay stack!).

### *2.2.5 DAQ and recording of the signals.*

The event builder architecture was deployed including DAQ computers (10 servers), storage (160 TB on disk and 100 TB on tape), networking (cabling, switches and fibres to control room & to external labs). The average electronic noise is measured to be well within expectations on practically all the 53720 channels: 1500 electrons rms to be compared with ~12000 free electrons produced by m.i.p. over 3 mm (S/N ≥ 8). An example of a m.i.p. — directly recorded from the collection signal — is shown in Figure 12.

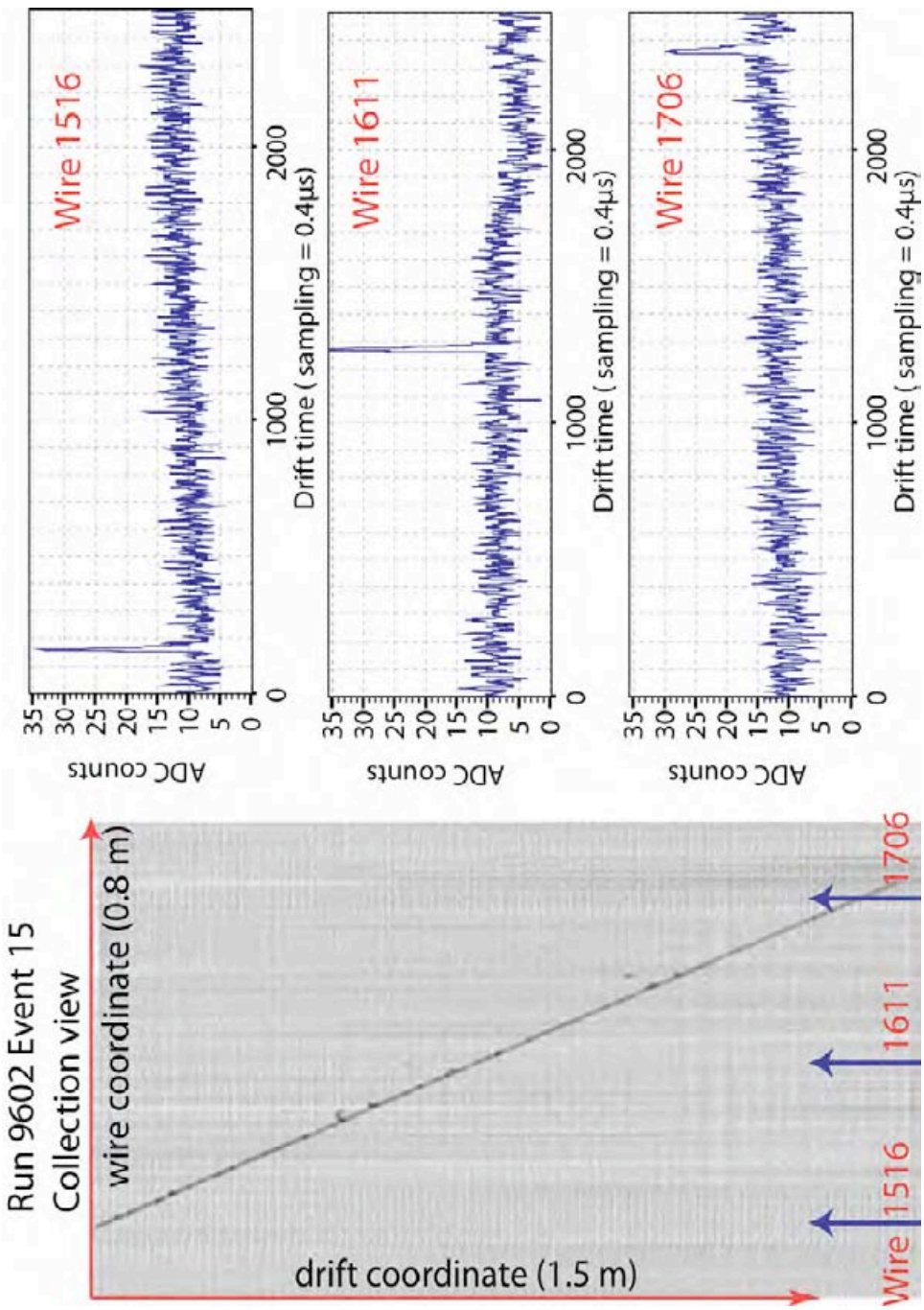


**Figure 12. Left:** Example of muon track crossing a 1.5 m full drift volume. **Right:** Signals recorded on single collection wires as a function of the drift time. The r.m.s noise is 1.5 ADC counts (1500 electrons equivalent), the pulse height is above 15 ADC counts (20000 electrons). The charge attenuation along the track allows a precise event-by-event measurement of the LAr purity.

The size of T600 full drift event is about 100 Mbytes, including lossless data compression. With the present limits of the data throughput, this corresponds to a maximum trigger rate of ~ 1 Hz. Multi-buffering scheme implemented in the DAQ allows the acquisition of trigger bursts with up to 8 events, without dead time.

In the forthcoming future the DAQ architecture will allow implementation of real-time zero skipping based on identification of regions of interest, reducing the amount of stored data. In turn, this would increase the sustainable trigger rate. Tests are underway to optimize the hit finding algorithms to the present noise level conditions. The CNGS beam early warning signals

used to generate a gate, within which the prompt scintillation light is used as global trigger.

A number of very impressive events have been observed during the present CNGS2 experiment, amongst which events due to cosmic rays and to the accelerated beam from the CERN-SPS. Typical beam related events are shown in Figure 10.

*2.2.6 Transport of the T600 from LNGS to CERN.*

The presently approved CERN physics programme foresees that there will be accelerator running during the whole 2012. This provides a useful and necessary time interval to perform the transport of the T600 from Assergi (L'Aquila) to CERN, in order ensure that the experiment can be made operational again in 2013. A preliminary analysis has shown that the operation of extracting the T600 from the underground laboratory is feasible within the existing configurations.

The two separable inner LAr containers (**7**) — where most of the inner mechanical structures are contained — are made of aluminium honeycomb, surrounded by frames of aluminium profiles and sandwiched between two aluminium skins. These panels are welded together to form a parallelepiped box ("T300" half-module) of relatively small external dimensions, 4.2 x 3.9 x 19.9 $m^3$. They have been entirely constructed and assembled in Pavia and subsequently transported sealed over the road to the Hall B of LNGS. It is therefore expected that the reverse operation from LNGS to CERN is possible as well.

Holes and chimneys (**11**) for the way out of signal cables of the internal detectors and control instrumentation, the ports (**14**) for LAr filling, gaseous Argon (GAr) recirculation and other services like vacuum instrumentation and safety disks have to be separated out and transported individually.

The two sub-modules are surrounded by a common thermal insulation layer (**10**), which is realised by evacuated Nomex$^{TM}$ honeycomb panels (0.4 m thick) to form a closed vacuum-tight box. These elements must be individually separated removing the local welding, transported and reconstructed again when in Hall B-191. Some replacements of these elements is necessary. A large number of additional components must also be separately disassembled in order to transport them from LNGS to CERN, including (1) the electronics for DAQ, (2) the cryogenic storages and auxiliary systems located in a dedicated "Service Area" composed by the three levels (floor, 5 m, 10m) of a supporting structure surrounding the T600 module and (3) the $LN_2$ liquefaction system.

# 3 The experimental setup at the CERN-PS.

*3.1 The CERN-PS beam.*

The proposed experiment will exploit the CERN-PS neutrino beam-line, originally used by the BEBC-PS180 Collaboration [28] and successively re-considered by the I216/P311 Collaboration [15]. The neutrino beam will be a low energy $\nu_\mu$ beam, centred at about 1 GeV, produced by 19.2 GeV protons, of intensity 1.25 $10^{20}$ pot/yr.

The CERN-PS can deliver routinely on a refurbished TT7 transfer line 3 $10^{13}$ protons per cycle at 20 GeV/c in the form of 8 equidistant bunches of approximately 60 ns during 2.1 $\mu$s. More than 1.25 $10^{20}$ pot/year can be collected by the experiment in one year of data taking for an optimal machine time availability. The actual beam sharing will depend on the extent of requirements from other users, in particular the n-TOF programme [29], even under the assumption of no major machine upgrade. The proton transfer line, the new target and the horn focussing system must be reconstructed.

As reference case the neutrino beam set-up used by the BEBC-PS180 $\nu_\mu \rightarrow \nu_e$ experiment has been chosen. An optimized design of new and possibly improved beam optics will be the subject of further studies. The 19.2 GeV/c proton beam is extracted from the PS and impinges on a 80 cm long, 6 mm diameter beryllium target. This is followed by a pulsed magnetic horn designed to focus positive particles of momentum around 2 GeV/c into a decay tunnel of about 50 m length. The tunnel cross section is 3.5 x 2.8 $m^2$ for the first 25 m of length and 5.0 x 2.8 $m^2$ for the rest of the length, allowing the decay of mesons with large angular divergence with respect to beam axis in the horizontal plane. The decay tunnel is followed by a 4 m thick iron shield and 65 m of earth to absorb the remaining hadrons and most of the muons (Figure 13).

Some preliminary studies about the realization of the TT7 PS neutrino beam line have been already completed at CERN. A detailed analysis of the beam modification has been approved by the CERN Management. Large parts of the required infrastructure are already available, but renovation may be needed. The TT7 transfer line the target chamber and the decay tunnel are in good shape and available for the installation of the proton beam line, target and magnetic horn. The target and secondary beam focusing design can be inspired form the CNGS experience as well as monitoring systems, primary beam steering and target alignment. Some important elements for the beam refurbishing, such as the main dipoles, quadrupoles, correction dipoles, the transformer for the magnetic horn, can be recuperated, reducing significantly cost and time schedule. For technical details we refer to Ref. [30].

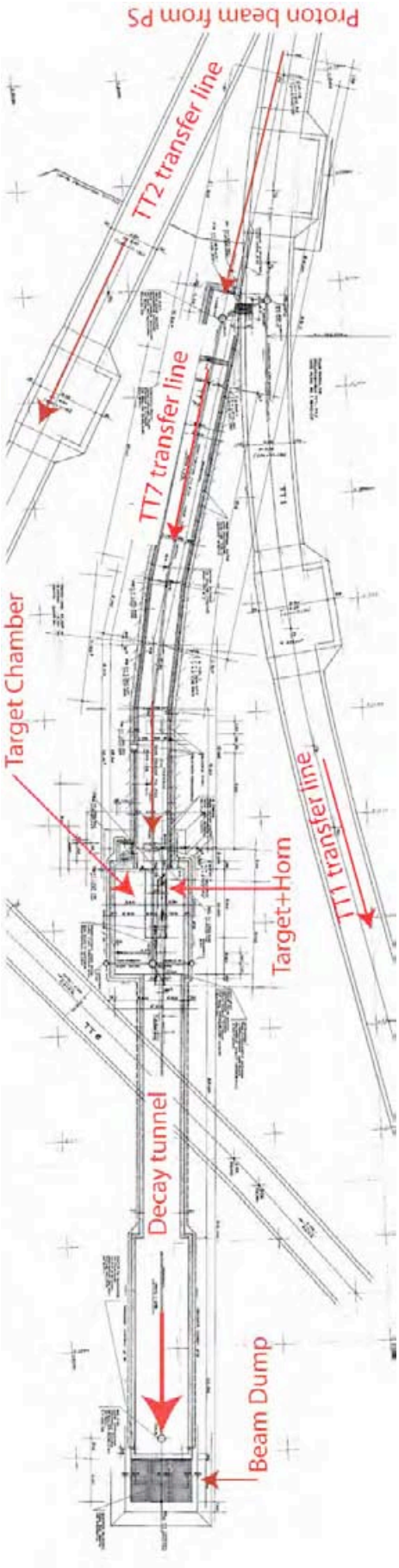


**Figure 13.** CERN-PS neutrino beam layout.

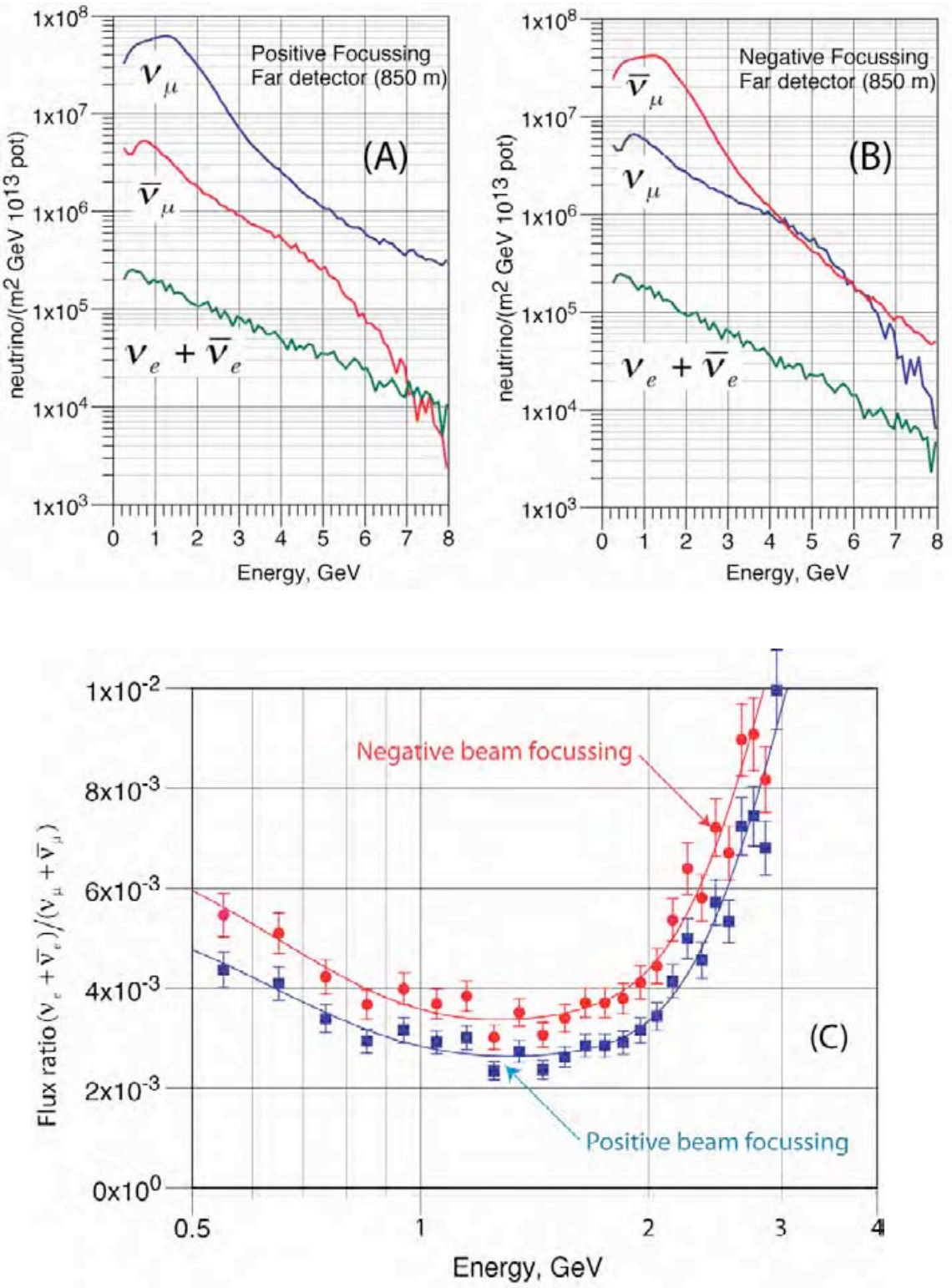


**Figure 14.** The expected CERN-PS neutrino (top-left) and antieutrino (top-right) beam fluxes in the far position. The corresponding ratio $(\nu_e+\bar{\nu}_e)/(\nu_\mu+\bar{\nu}_\mu)$ is also shown (bottom).

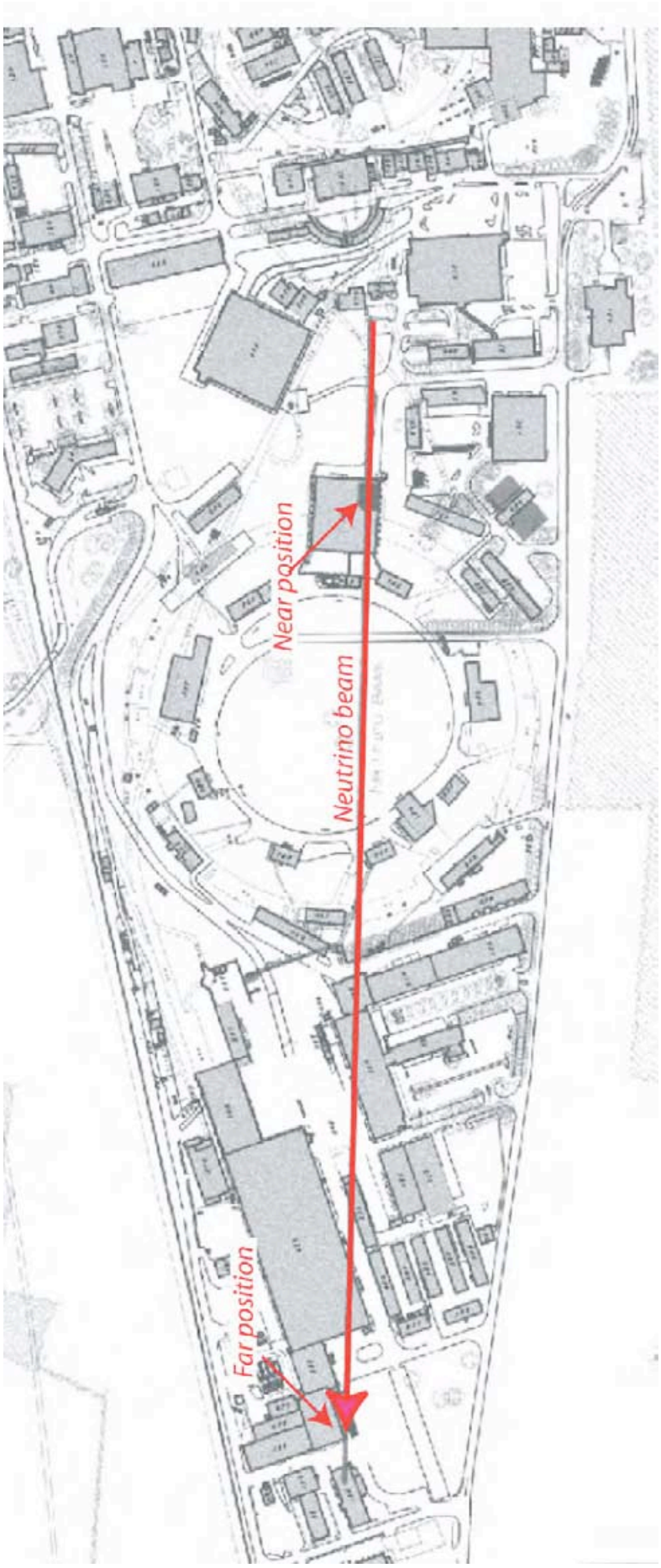


**Figure 15.** Neutrino beam from the CERN-PS. Two locations, respectively at 850 and 127 m from the target are simultaneously recorded in order to evidence possible oscillation effects.

The available beam intensity to be dedicated to the neutrino beam is strongly dependent on the actual proton beam sharing with other users. The total accumulated number of accelerated protons from the PS in 180 days of operation is today about ~ 3.6 $10^{20}$ p.o.t./year. With one third of the protons dedicated to the neutrino beam line, the expected intensity will be about 1.25 $10^{20}$ p.o.t./year. Such a target value has also been already assumed for the previously proposed I216/P311 experiment.

The positively and negatively focussed CERN-PS neutrino spectra, originally used by the BEBC-PS180 Collaboration, are shown respectively in Figure 14A and 14B for the most relevant "Far" position at 850 m from the PS target; the corresponding $(\nu_e + \bar{\nu}_e)/(\nu_\mu + \bar{\nu}_\mu)$ flux ratio as a function of the incoming neutrino energy is shown in Figure 14C. We remark that flux ratios for negative and positive focussing are very similar and about 20% larger in the case of the anti-neutrino focussing.

The two closely similar LAr-TPC's will be located respectively at 850 m and 127 from the PS target (Figure 15) in the existing locations B191 and B181 respectively. The size of the buildings is perfectly adequate and no major civil engineering is needed. The two detectors are perfectly lined up with the direction of the neutrino beam, although a very slight adjustment of the direction of the horn may be needed.

The operation of the CNGS2 detector was obviously underground. However the T300 test in Pavia has demonstrated that the LAr TPC detectors can operate safely as well on surface, as required by the present experimental proposal. In particular space charge effects due to the presence of a much larger cosmic ray background have been demonstrated to be entirely acceptable.

*3.2 The "Far" detector.*

The T600 detector is to be operated at CERN without major modifications, the only difference being the average energy of the neutrino beam, which is in the region of 1-2 GeV. This will introduce significant simplifications in the data analysis with respect of the CNGS2 where the average neutrino energy is about 20 GeV. These events are therefore much easier to analyze and they resemble on one hand to the Gargamelle events and on the other side to the cosmic neutrino events, with the additional advantage that the direction of the incoming neutrino is well known. Most of the events, including the muon tracks are now fully contained.

The old BEBC experimental hall (Bdg. 191) is fully adequate to host the T600 as "Far" detector for the proposed experiment (Figure 16). The useful surface is about 26 x 45 $m^2$ and the height is more than 20 m. The clearance of the entrance doors is 16 m height and 10 m width.

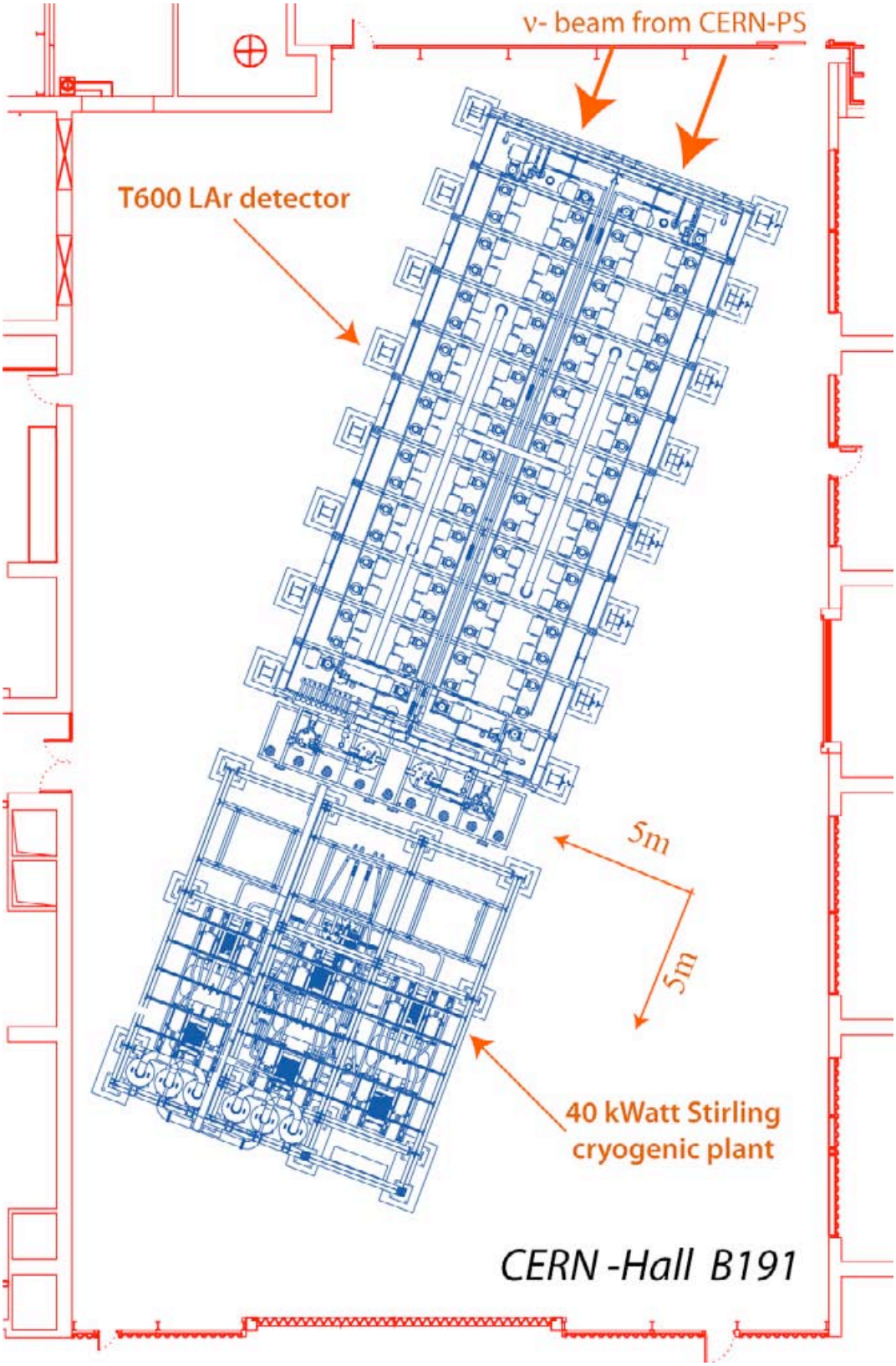


**Figure 16.** The general layout of the T600 LAr detector in the "Far" Position and of the associated cryogenic equipments in Hall B-191 at CERN. The direction of the neutrino beam is also indicated.

The hall is equipped with two cranes (170 t and 5 t each) placed at 16 m height spanning the whole surface. Electrical power and cooling are also available.

As in the case of LNGS, the insulation vessel has to be realized in situ. Solutions could be envisaged based on the experience developed by the collaboration during the construction of the T600 at LNGS. The most obvious solution is to take along the already constructed Nomex insulation panels. We remark however that some of these panels are not within specifications and they must be replaced. Therefore the availability of new commercial material well suited and tested for our purposes, may allow increasing the insulation efficiency, relying only on simple passive scheme. Consequently the present evacuated honeycomb panels may be replaced with layers of readily available Divinycell H material, which requires no vacuum (hence no pressure forces) with a thermal conductivity of 0.030 W/(m K). Using a thickness of about 1 m, the expected heat loss rate should be well below the present 10 $W/m^2$.

Alternatively, it could be realized with 1 m perlite walls (thermal conductivity of 0.029 W/m/K) on the four sides and on the top. The bottom wall could be realized with low conductivity bricks, also about 1 m thick.

Under any circumstance, a reliable and efficient insulation vessel could be realized at CERN in a relatively short time.

### *3.3 The "Near" detector.*

While the "Far" detector is relying on the already existing T600, the "Near" detector must be constructed anew. In order to ensure the maximum similarity between the two detectors, required in order to ensure identical behaviours in absence of time dependent oscillations, the "Near" detector design will be as far as possible identical to the T600 "Far" detector except the total mass which has been conservatively chosen to be of 150 t, namely a clone of a single T300 half-module with the length reduced by a factor 2 (about 12 m). This allows keeping untouched the inner detector layout (Figure 17).

The detector dimensions including 1 m passive insulation similar to the one to be used in the "Far" detector. will be 13 x 6 $m^2$ with a height of 6 m. It is a fortunate circumstance that with an area of 17 x 10 $m^2$ and a height exceeding 6 m (Figure 18) the already existing basement pit of hall B-181, previously used for neutrino oscillation experiments, fits perfectly the "Near" detector. The neutrino beam crosses the pit at a height of about 3 m above the floor. Electronic racks will be installed on top of the detector at floor level. A surface of about 10 x 10 $m^2$ is required to locate the cryogenic equipments close to the detector pit.

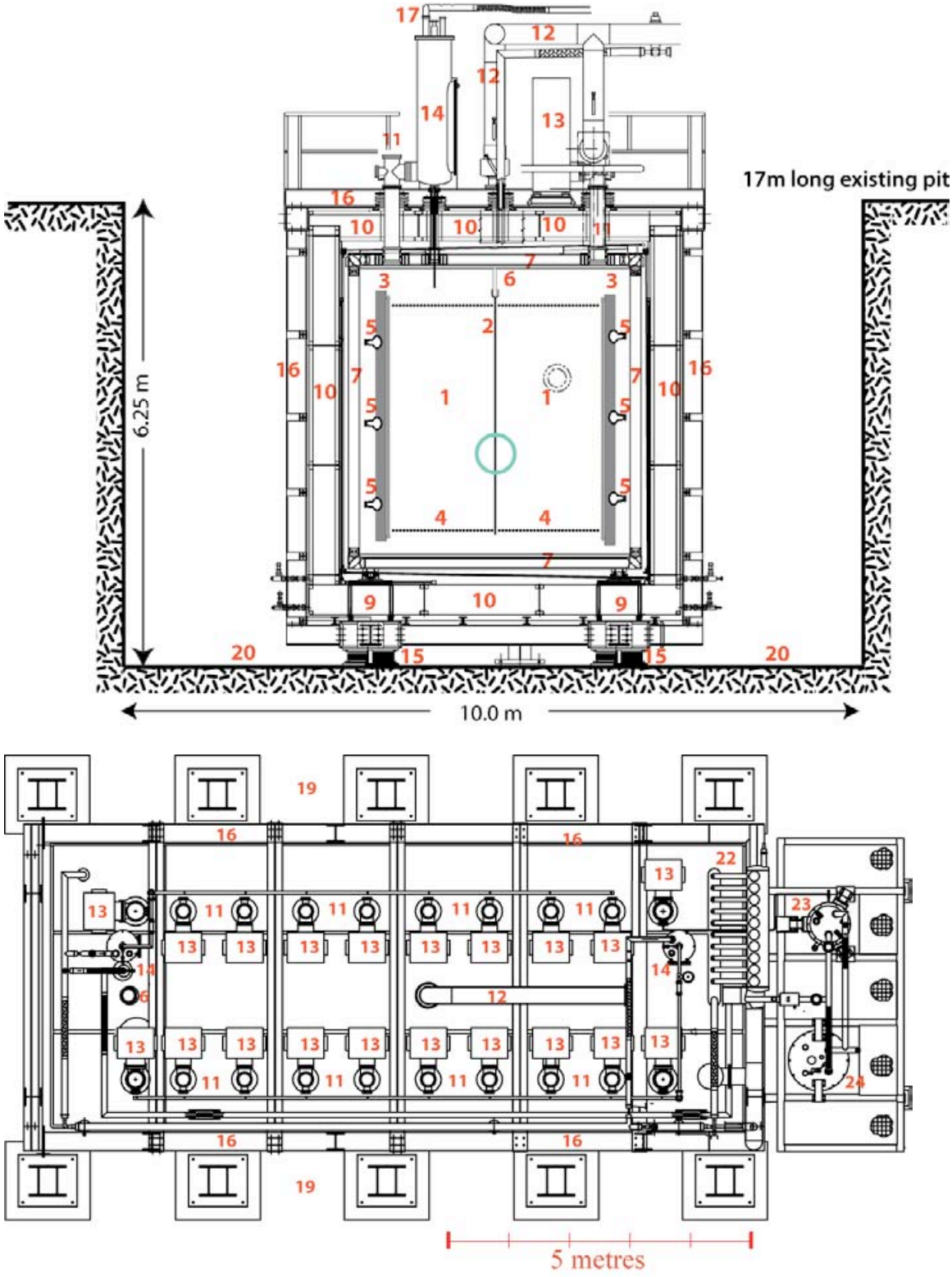


**Figure 17.** Technical drawings of the T150 near detectors. Vertical cross-setcion (top) and top view (bottom) are shown. Numbered items are explained in the text.

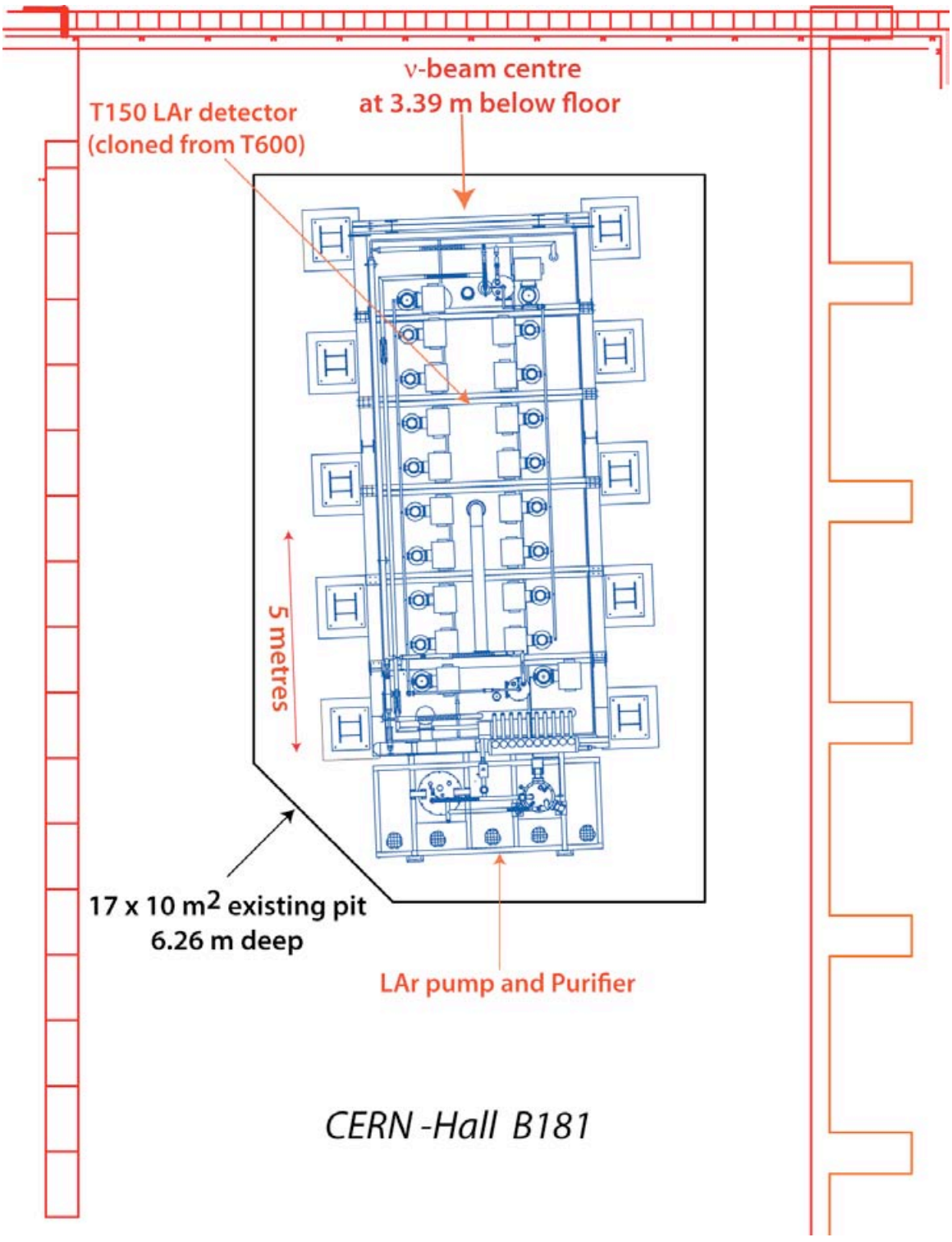


**Figure 18.** General layout of the new T150 LAr detector "cloned" from the ICARUS detector in the Close Position in Hall B-181 at CERN.

In particular, the wires, of a maximum length of about 10 m, will be anchored by special holders onto the wire frame in groups of 32 units (the wire modules). Only one set of horizontal wires (1056 units), about 10 m long, forms the induction-1 plane, stretched between the vertical beams of the wire frame; in both the induction-2 and collection planes (wires inclined at ±60°) the standard length of the wires stretched between the upper and lower beams of the frame will be 3.77 m (~1900 wires per plane), while wires of decreasing length (960 wires per plane) will be used in the triangular-shaped portions, between one vertical and one horizontal beam, at the corners of the planes. Obviously the number of wires in the "Near" detector will be about ¼ of the ones of the existing T600.

All the other component of the detector, cryogenic elements, internal photomultipliers, front-end electronics and read-out system, DAQ and ancillary equipments, will have to be replicated keeping in mind of the down-scaled detector mass: one GAr recirculation system (**14**), one LAr recirculation system (**23**, **24**), two LN2 recondenser units (**21**, **22**), 14200 electronic channels with 25 electronic racks (**13**) and 30 PMT's of 8" diameter and related electronics (**5**).

Of course some obvious improvements and some simplifications over the by now 10 years old T600 may be implemented with the new detector.

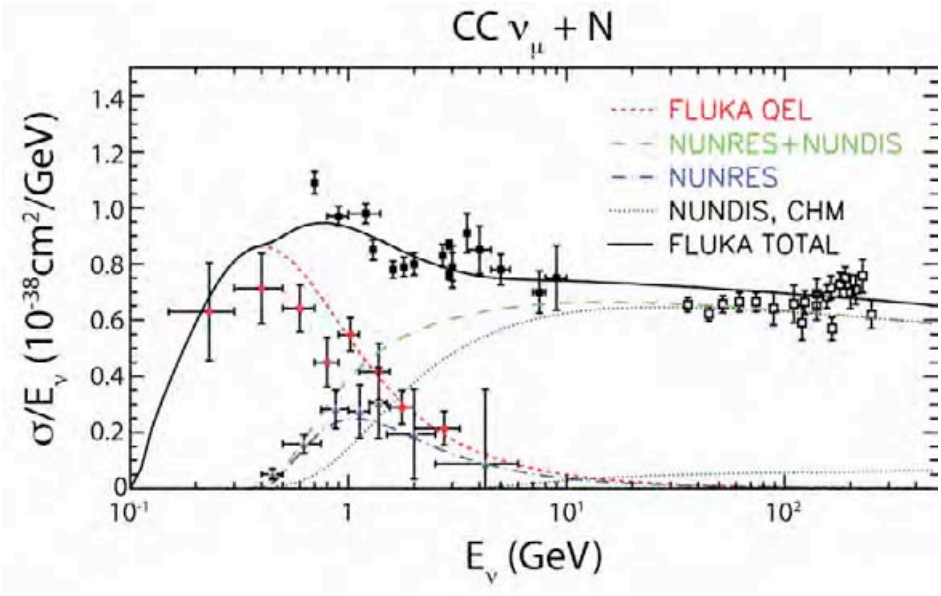


**Figure 19.** Total cross section for CC $\nu_\mu$-N interactions as a function of the incident neutrino energy. The various contributions from the FLUKA calculations are explained in the figure. Charm production is displayed separately, but is part of the NUNDIS event generator. Refer to [35] for details on experimental data.

# 4 Signal selection and background rejection.

In the LAr-TPC all reaction channels with electron production can be analyzed without the need to restrict the search to the quasi-elastic channel, which accounts for about one half of the events (Figure 19). Moreover, events due to neutral currents are also very well identified and can be rejected to a negligible level.

The energy resolution and detector granularity are largely adequate for the lower energy range (1 ÷ 3 GeV) relevant for the present proposal.

The performance of the LAr-TPC has been extensively studied in the 2001 T300 technical run with cosmic rays [27]. Electromagnetic energy resolution is $\sigma(E)/E = 0.03/\sqrt{E(GeV)} + 0.01$, in agreement with $\pi^0$ invariant mass measurements in the sub-GeV energy range. At higher energies the estimated resolution for hadronic showers is $\sigma(E)/E = 0.30/\sqrt{E(GeV)}$. However the LAr-TPC detector allows to identify and measure, track by track, each hadron produced in ~1 GeV neutrino interactions, through ionization and range, leading to a much better energy resolution. In fact most of the particles, generated in the neutrino interactions, come to rest within the detector, including muons.

A number of physical features the LAr-TPC, relevant for the present proposal, as obtained from the experimental data, are shown in Figure 20 (A to F).

The integrated energy loss of cosmic ray stopping muons can be directly compared with the momentum determined by multiple scattering. The Kalman filter method has been used, applied to segmented tracks ($L_{seg}$ = segment length). The resulting momentum was then extracted from the deflection angle $\theta$ and from $\chi^2$ of the fit. A resolution $\Delta p/p=15\%$ due to multiple scattering [31] has been obtained for energies up to 0.5 GeV (Figure 20.A). The procedure, thus validated, has been extended to higher energy with MC calculations; the resolution $\Delta p/p$ can be as good as 10%, depending mainly on track length (Figure 20.B).

The measured $dE/dx$ energy losses for pions and protons are shown in Figure 20.C. Clear separation of the nature of the particle is easily obtained from the last part of the residual range.

In Figure 20.D we report the excellent resolution obtained from the decay electron spectrum (Michel parameter) from muon decays, collected from the T300 technical run exposure [32]. The bremsstrahlung losses have been included.

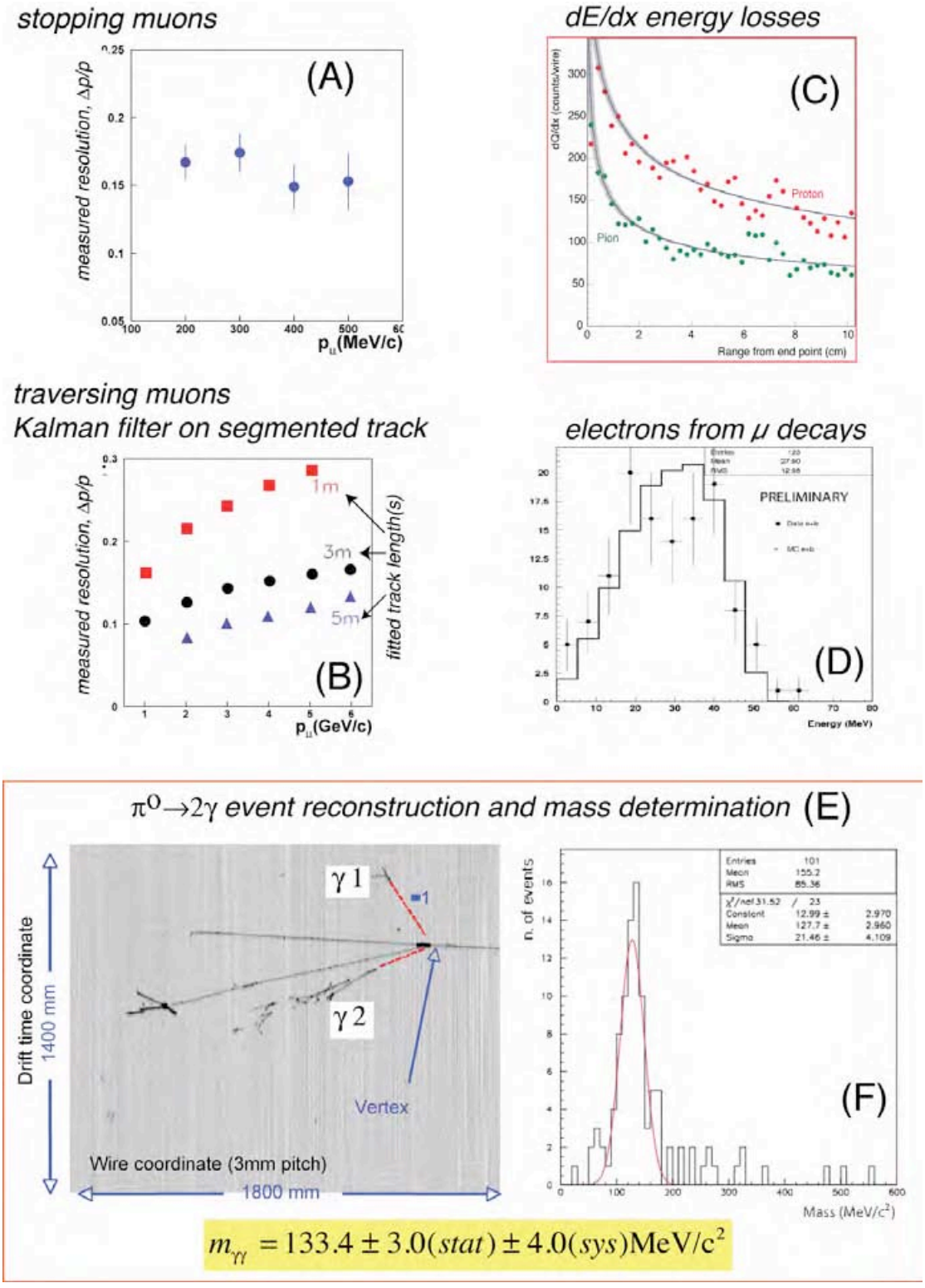


**Figure 20**. Experimental results from the T300 Pavia ICARUS run (A) momentum resolution of stopping muons; (B) momentum resolution of traversing muons with the Kalman filter method; (C) dE/dx energy loss for slow pions (green) and protons (red); (D) Michel electron decay spectrum from $\mu \rightarrow$ e decays; (E) $\pi^{o} \rightarrow 2\gamma$ event reconstruction and mass determination; and (F) mass spectrum of 230 interactions with $\gamma\gamma$ candidates

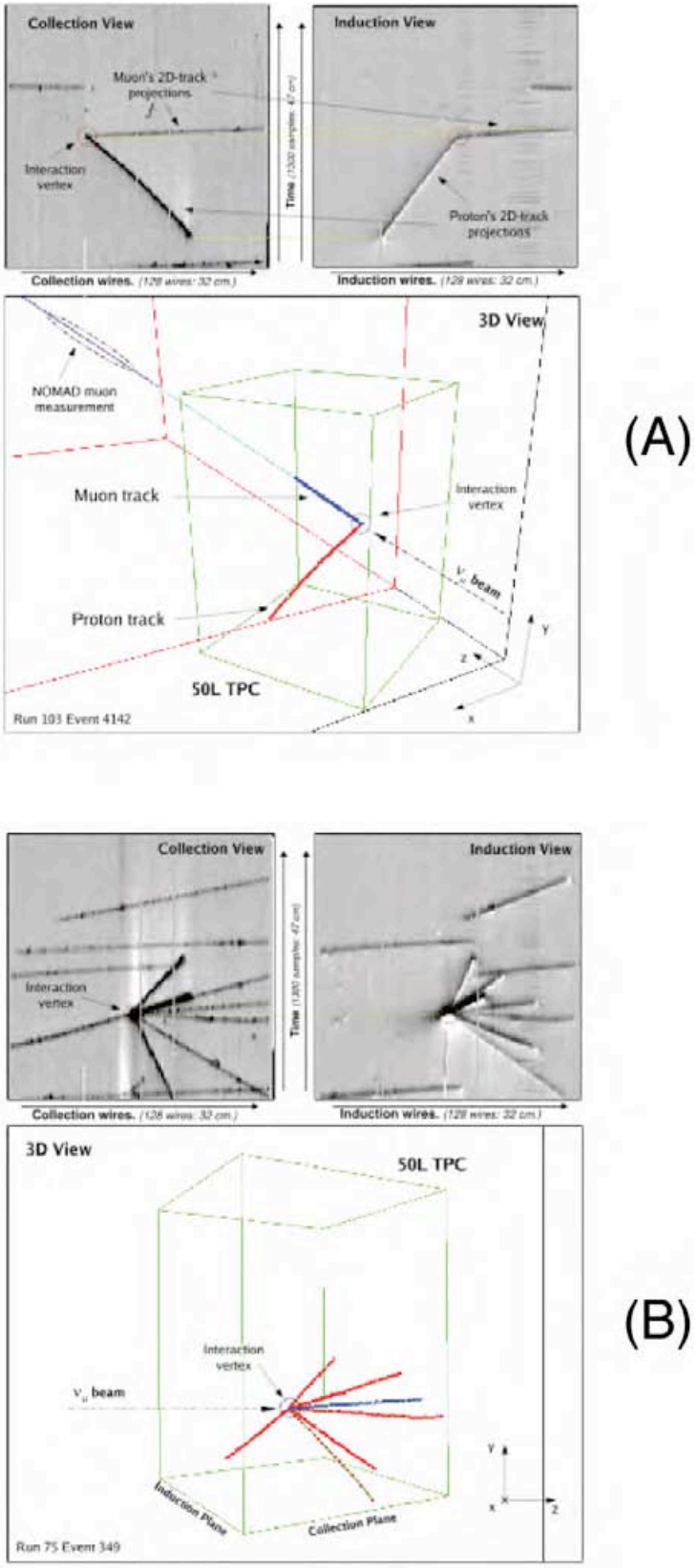


**Figure 21.** Events from a 50 litre ICARUS TPC exposed to the CERN-SPS neutrino beam in coincidence with the NOMAD experiment: (A) a quasi–elastic event with a muon and a proton recoil track; (B) a complex multi-hadron event. In both events a 3D reconstruction is shown.

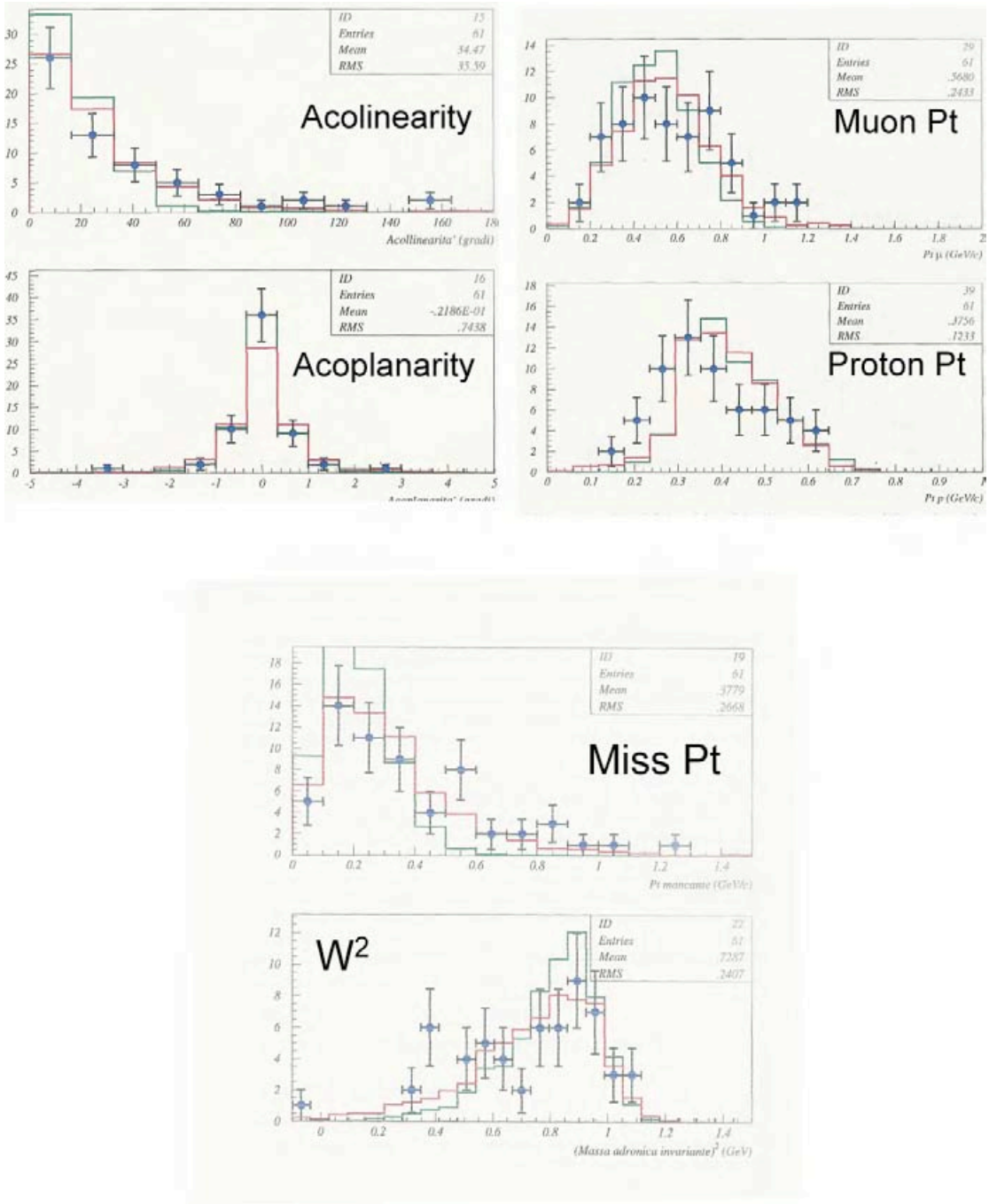


**Figure 22.-** Selection of ~ 200 pure lepton-proton quasi elastic final state with exactly one proton $T_P$>50 MeV (range > 2 cm) and any number protons $T_P$<50 MeV. Good agreement with FLUKA expectations (Red line), accounting for Nuclear Fermi motion and re-interactions in nuclei.

The reconstruction of a typical $\pi^0 \rightarrow 2\gamma$ event from the T300 technical run is shown in Figure 20.E; both $\gamma$ 's converting away from the hadronic vertex have been identified, associated and measured. Finally in Figure 20.F we show the 230 hadronic interactions with $\gamma\gamma$ candidates selected from T300 Pavia run. A prominent $\pi^0$ peak is found with an invariant mass of 133.4 ± 3.0± 4.0 MeV/$c^2$ [33]. The corresponding $\gamma$ conversion length is (17.4 ± 0.8) cm, in agreement with the expectation of 18 cm.

Quasi-elastic neutrino events in LAr have been reconstructed in the 50 litre ICARUS LAr-TPC exposed to the CERN-WANF beam in coincidence with the NOMAD experiment [34]. In Figure 21 two events are shown: (A) a quasi-elastic proton recoil event, a typical topology of the present Proposal as well; (B) a multi-prong event. Both events can be readily reconstructed in 3D with particle identification, momentum balance and $\pi^0$ rejection. We notice that in this exposure only two views were available, and the reconstruction will be easier with the three views of the present T600.

Finally in Figure 22 we present a selection of ~ 200 pure lepton-proton final state events from the 50 litre ICARUS LAr-TPC with exactly one proton $T_P > 50$ MeV (range > 2 cm) and any number protons $T_P < 50$ MeV. There is a good agreement with FLUKA expectations, accounting for Nuclear Fermi motion and re-interactions in nuclei [22].

A full simulation of the expected neutrino events in the LAr detectors for the proposed experiment has been performed within the FLUKA framework [35], where all interactions are included. It must be stressed that especially at low energies the corrections due to the nuclear effects and Pauli exclusion principle are substantial [36]. However, these effects are the same and therefore cancel out when the spectra in the "Near" and "Far" positions are compared.

In Figure 23 we show a $\nu_e$ CC interaction for 1.5 GeV neutrino. The Monte Carlo simulation shows that the energy reconstruction of electron neutrino interaction events is not affecting the signal/background ratio if a minimal cut of 50 cm in the longitudinal direction and a 10 cm cut on the sides of the sensitive volume are performed, corresponding to a fiducial volume of about 90 % of the active one. Electron identification is also ensured under these geometrical cuts. Indeed, due to the directionality of the neutrino beam, the probability that an electron escapes from the instrumented volume before initiating a shower is extremely small: only 2 % of the electrons travel through a LAr-TPC thickness smaller than 3 $X_0$ and 0.3 % travel less than 1 $X_0$ in the instrumented volume. With the previously described fiducial volume cuts, the expected average neutrino energy resolution is about 14%.

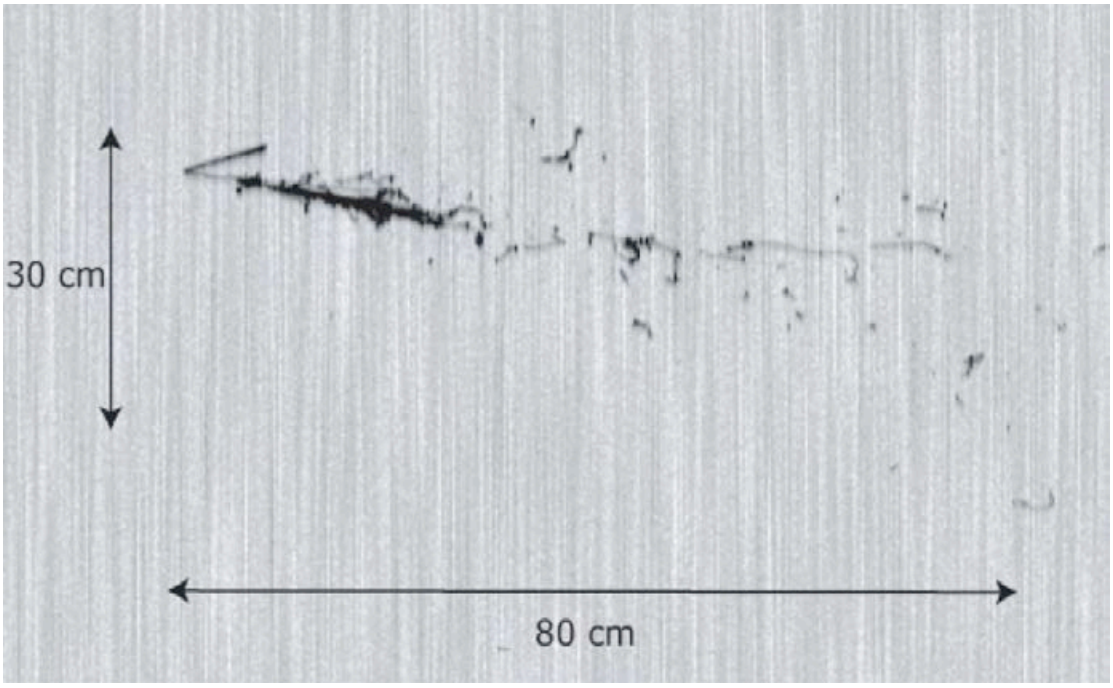


**Figure 23.** Collection view of a 1.5 GeV QE electron neutrino event. Note the presence of a singly ionizing electron immediately after the event.

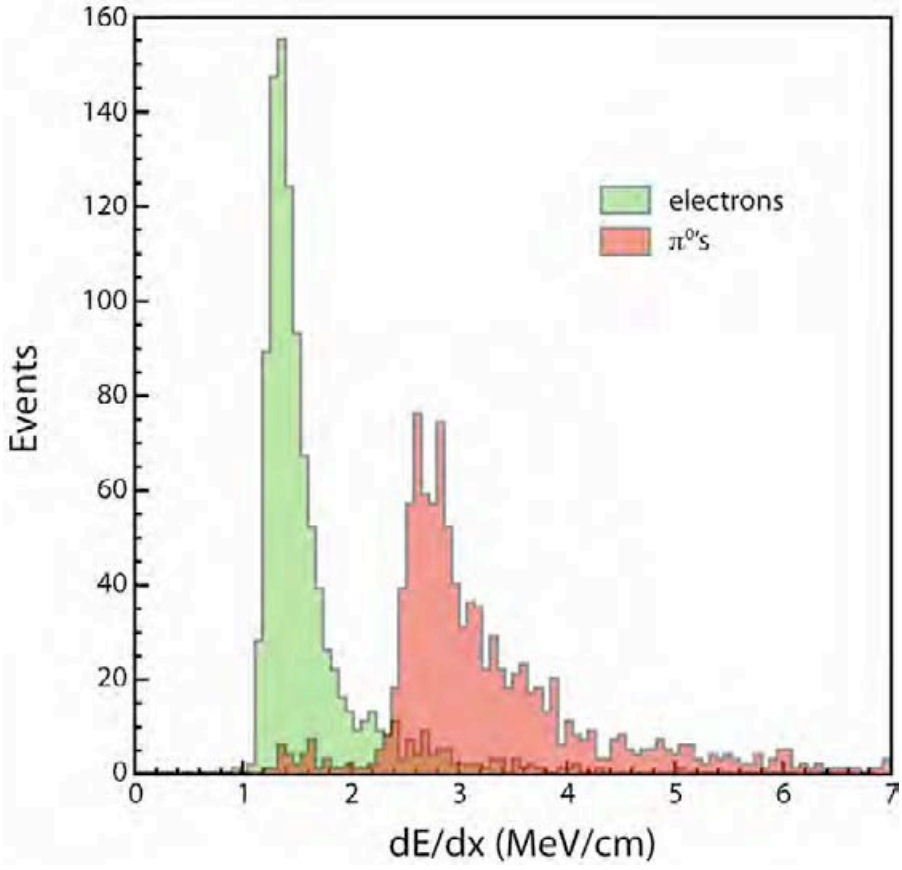


**Figure 24.** Electron-$\pi^0$ separation obtained in the LAr-TPC using ionization measurements along tracks in the vertex region.

In view of the excellent imaging capability of LAr-TPC, $\pi^0$ from $\nu_\mu$ NC events cannot be misidentified as electrons because all events, where both photon conversion points can be distinguished from the $\nu_\mu$ interaction vertex, can be rejected. In the analysis photons converting at more than 2 cm from the $\nu_\mu$ vertex were rejected. The remaining $\pi^0$ background is further reduced by discarding events where the parent $\pi^0$ mass can be reconstructed within 10 % accuracy. Only 3 % of $\pi^0$ survives the cuts for events with vertexes inside the fiducial volume. The remaining photons can be discriminated from electrons on the basis of dE/dX analysis. This method provides 90 % electron identification efficiency with photon misidentification probability of 3 %. The final $\pi^0$ mis-interpretation probability is 0.1 %, the corresponding electron neutrino detection efficiency is 90 % within the fiducial volume (Figure 24).

As an important feature of the present proposal, the possibility to run with anti-neutrino beam has been considered in order to further check the LSND claim, which is mainly based on anti-neutrino data. Switching the horn polarity to select negative sign mesons results in an anti-neutrino beam with total fluence of 68 % with respect to the neutrino mode and a similar energy spectrum. For the anti-neutrino oscillation search, the full simulation will be available soon. The expected event rate has been calculated by folding the flux spectra of Figure 14 with the relevant anti-neutrino cross sections. The resulting event rate is 17 % of that collected in neutrino mode. This reduction is due to the larger impact of nuclear effect on the anti-neutrino interactions, where the momentum transfer is smaller.

**Table 5**. Event rates for the "Far" and "Near" detectors given for 2.5 $10^{20}$ pot for $E_\nu < 8$ GeV. Neutrino fluxes are taken from Ref. [15]. The oscillated signals are clustered below 3 GeV of visible energy.

| | $\nu$ focus | | $\bar{\nu}$ focus | |
|---|---|---|---|---|
| | FAR | NEAR | FAR | NEAR |
| Fiducial mass | 500 t | 150 t | 500 t | 150 t |
| Distance from target | 850 m | 127 m | 850 m | 127 m |
| $\nu_\mu$ interactions (or $\bar{\nu}_\mu$ for $\bar{\nu}$ focus) | 1.2 x $10^6$ | 18 x $10^6$ | 2.0 x $10^5$ | 2.3 x $10^6$ |
| QE $\nu_\mu$ (or $\bar{\nu}_\mu$) interactions | 4.5 x $10^5$ | 66 x $10^5$ | 87000 | 1.0 x $10^6$ |
| Events/Burst | 0.17 | 2.5 | 0.03 | 0.3 |
| Intrinsic $\nu_e + \bar{\nu}_e$ from beam | 9000 | 120000 | 2000 | 29000 |
| Intrinsic $\nu_e + \bar{\nu}_e$ ($E_\nu < 3$ GeV) | 3900 | 54000 | 880 | 13000 |
| $\nu_e$ oscillations: | | | | |
| $\Delta m^2 = 2.\ eV^2;\ sin^2 2\theta = 0.002$ | 1194 | 1050 | 230 | 58 |
| $\Delta m^2 = 0.4\ eV^2;\ sin^2 2\theta = 0.02$ | 2083 | 2340 | 330 | 115 |
| $\Delta m^2 = 0.064\ eV^2;\ sin^2 2\theta = 0.96$ | 3350 | 1250 | 465 | 140 |
| $\Delta m^2 = 4.42\ eV^2;\ sin^2 2\theta = 0.0066$ | 2980 | 25050 | 490 | 3220 |

Because of the same reason, the $\nu_\mu$ component is strongly enhanced. Event rates in the CERN-PS beam for the un-oscillated spectra and a few $\nu_\mu \leftrightarrow \nu_e$ oscillation values are reported in Table 5.

An important feature of the present proposal is the large statistics of neutrino interactions which can be collected. This is possible by the LAr-TPC detection technique, which allows the reconstruction of the totality of neutrino interactions without restricting to the QE interactions and to realize absolutely homogeneous detector of large mass. The adopted neutrino beam energy permits, unlike lower energy beams, to obtain useful neutrino rates, also operating in antineutrino mode.

## 5 Sensitivity to $\nu_e$ and $\nu_\mu$ disappearance signals.

As already described, our proposal at the CERN-PS is based on the search for spectral differences of electron like specific signatures in two identical detectors, 850 m and 127 m away from the source. The choice of these two distances is related to the persisting presence of the disappearance anomalies in the $\left|\sin^2_{new}\right| - \left|\Delta m^2_{new}\right|$ plane for a sterile neutrino hypothesis of reactor neutrino experiments, Gallex and Sage calibration sources and other experiments. As well known, these data may be well fitted by the 3 + 1 neutrino hypothesis, while the no-oscillation hypothesis is disfavored at 99.93% C.L. The presently proposed experiment is however intended to detect experimentally the oscillation pattern and not simply the so far unaccounted lack of $\nu_e$ events. Both the $\nu_e$ and $\nu_\mu$ disappearance signals may be searched for.

The signal produced by 19.2 GeV protons can be hereby tuned separately to neutrinos or antineutrinos. Important unaccounted differences are being hinted between these two neutrino species which may even be related to a failure of CPT symmetry.

The $\nu_e / \bar{\nu}_e$ beam components are produced by the three body decays of K and μ. As shown in Figure 5, the spectral distributions are extremely similar. The intensity of the $\nu_e$ signal is however much smaller than the one of the dominant $\nu_\mu$'s (about 0.5%), however largely sufficient in order to collect an adequate number of events. The signature of charged currents $\nu_e$ events is extremely clean because of the unique "bubble chamber like" quality of the events produced by the LAr-TPC enhanced by the close similarity of the two detectors.

In absence of oscillations, after some beam related small spatial corrections, the two energy spectra should be a precise copy of each other. An exact proportionality between the two $\nu_e$ spectra implies directly the absence of neutrino oscillations. Any experimentally observed $\nu_e$ difference between the rates of events at the two locations must be inevitably attributed to a time evolution of the neutrino species.

In Figure 25 the energy distributions of the electron neutrino events is shown in (a) and (b) respectively for the "Far" and "Near" and a number of possible $\left|\Delta m^2_{new}\right|$ value in the region of > 1eV$^2$ and $\sin^2(2\theta_{new}) \approx 0.16$. If confirmed without any doubt such a large mass difference will have an important role in the explanation of the existence of the Dark Mass in the Universe.

In Figure 26 the 90% confidence levels for the actual oscillation mechanism in the $\left|\sin^2_{new}\right| - \left|\Delta m^2_{new}\right|$ plane are shown for the presently proposed experiment with an integrated intensity corresponding to (a) 2.5 x $10^{10}$ POT (protons on target) for the original beam intensity of about 30 kWatt of the previous CERN/PS experiments, (b) to 7.5 x $10^{10}$ POT for the newly planned

90 kWatt neutrino beam at CERN/PS and (c) a 270 kWatt curve. They are also compared with the "anomalies" from the combination of the published reactor neutrino experiments, Gallex and Sage calibration sources experiments.

The disappearance signal in the same $\left|\sin^2_{new}\right| - \left|\Delta m^2_{new}\right|$ range may also be studied independently with the dominant $\nu_\mu$ and $\bar{\nu}_\mu$ signals. We remark that the $\nu_\mu \to \nu_{new}$ process has a different and independent signature than the one due to explicit $\nu_\mu \to \nu_e$ oscillations related to LNSD/MiniBooNE anomalies. However the $\nu_\mu$ and $\bar{\nu}_\mu$ spectral shapes, hereby primarily due to pion decays, are significantly different in the "Near" and "Far" positions. In the energy range below 3 GeV, where the effect is expected, the relative differences amount to about 30% and they may be predicted to about 1%, which is larger than what expected from the huge available statistics but quite significant for a test. The presence of the two alternate phenomena presumably with different values of $\sin^2(2\theta_{new})$, if confirmed, will hint at the presence of an appropriate fourth neutrino mass matrix $U_{4,k}$ with k = $\mu$ and e.

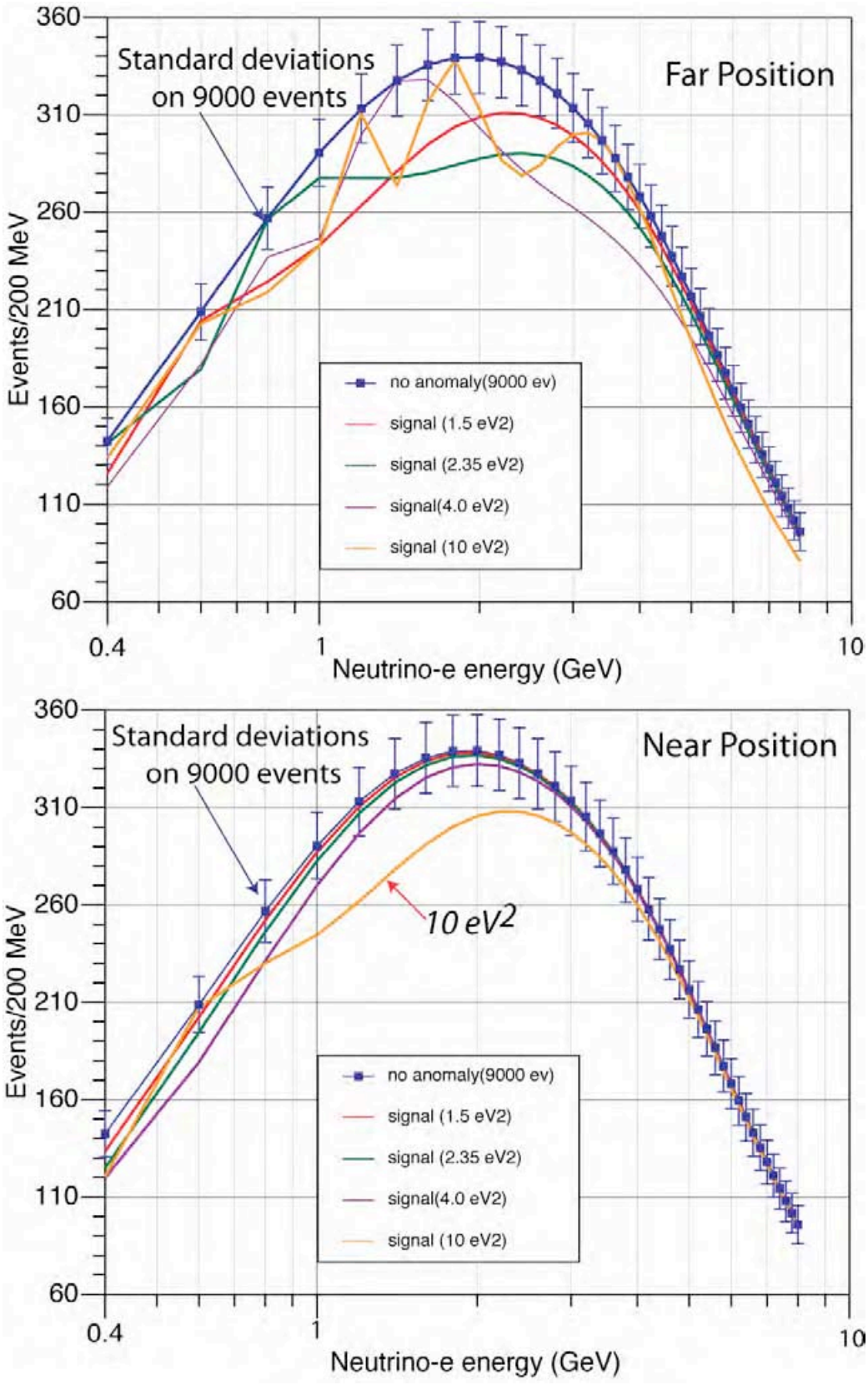


**Figure 25.-** Energy distributions of the electron neutrino events in (a) and (b) respectively for the "Far" and "Near" and a number of possible $|\Delta m^2_{new}|$ value in the region of > 1eV$^2$ and $\sin^2(2\theta_{new}) \approx 0.16$.

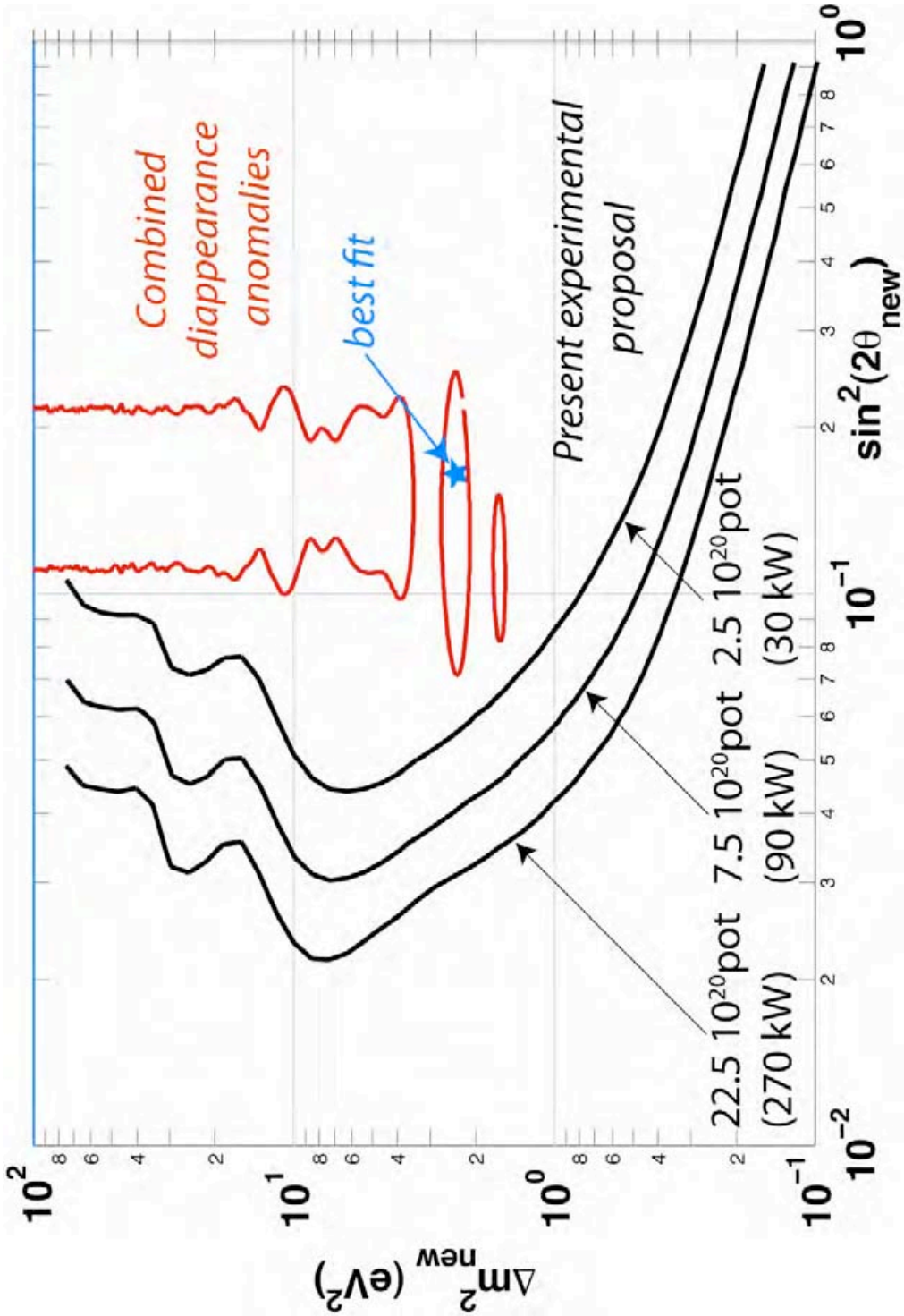


**Figure 26**.- Actual oscillation sensitivity (90% confidence level) in the $\sin^2(2\theta_{new})$ vs. $\Delta m^2_{new}$ distribution and for an integrated intensity of (a) $2.5 \times 10^{10}$ POT (protons on target) at the 30 kWatt beam intensity of the previous CERN/PS experiments, (b) to $7.5 \times 10^{10}$ POT for the newly planned 90 kWatt neutrino beam and (c) a 270 kWatt curve. They are compared (in red) with the "anomalies" from the combination of the published reactor neutrino experiments, Gallex and Sage calibration sources experiments. A 1% overall and 3% bin-to-bin systematic uncertainty on the energy spectrum is included (for 100 MeV bins).

# 6 Sensitivity to $\nu_\mu \rightarrow \nu_e$ Oscillations.

A sensitivity of $\sin^2 2\theta < 3\ 10^{-4}$ (for $\Delta m^2 < 2\ eV^2$) and $\Delta m^2 < 0.02\ eV^2$ (for $\sin^2 2\theta = 1$) at 90 % C.L. is expected with a two year exposure at the CERN-PS $\nu_\mu$ beam (Figure 27A). The parameter space region allowed by the LSND experiment is fully covered, except for the highest $\Delta m^2$ region. The sensitivity has been computed assuming a 3% systematic uncertainty in the "Far" to "Near" ratio prediction.

In anti-neutrino focusing, twice as much exposure ($5.0\ 10^{20}$ pot) allows to cover both the LSND region and the new MiniBooNE results (Figure 27B). Both favoured MiniBooNE parameter sets, corresponding to two different energy regions in the MiniBooNE antineutrino analysis, fall well within the reach of this proposal.

In Figure 28 a number of experimentally expected oscillation patterns at 850 m are shown for two neutrino (mu - e) oscillations and for some indicative positions of the LSND allowed region (indicated with a star mark). One can see that very different and clearly distinguishable patterns are indeed possible depending on the actual values in the ($\Delta m^2 - \sin^2 2\theta$) plane. It appears that the present proposal, unlike LSND and MiniBooNE, can indeed determine in the case of an observed effect, both the mass difference and the value of the mixing angle. In Figure 28 the intrinsic $\nu_e$ background due to the beam contamination is also shown. The magnitude of the expected oscillatory behaviour, although for the moment completely unknown, is in all circumstances well above the background, also considering the very high statistical impact of the experimental measurement.

As an additional bonus, the large statistics of excellent quality data will also profit to the knowledge of neutrino cross-sections. Precise measurements of the neutrino cross-section in the 0-5 GeV energy range are required by present and future neutrino oscillation experiments. Existing data on charged current quasi-elastic, deep inelastic, and single pion production are affected by a large uncertainty, especially at the lower energies [37]. Owing to the very low detection threshold of the Liquid Argon technique, the exposure at the CERN-PS neutrino beams could significantly improve the neutrino cross-section knowledge. Approximately $1.2\ 10^6$ and $1.8\ 10^7$ charged current events per $2.5\ 10^{20}$ pot will be recorded from the CERN-PS in the "Far" and "Near" detectors respectively, with a neutrino spectrum peaked at around 1 GeV. Neutral current cross-sections are also measured, with approximately $4.4\ 10^5$ and $6.0\ 10^6$ events in the "Far" and "Near" detectors respectively.

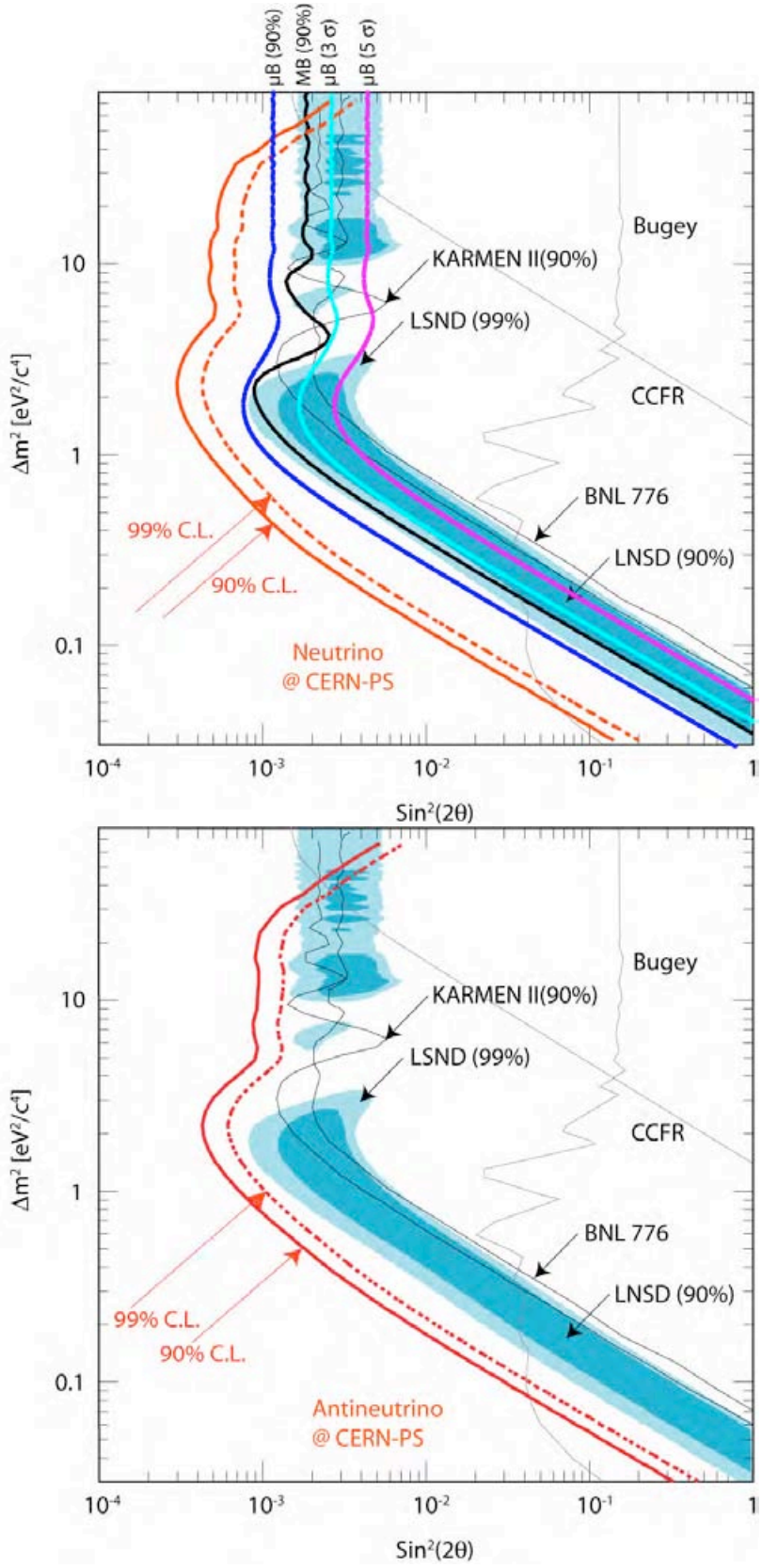


**Figure 27.** Expected sensitivity for the proposed experiment exposed at the CERN-PS neutrino beam (top) and anti-neutrino (bottom) for 2.5 $10^{20}$ pot and 5.0 $10^{20}$ pot respectively. The LSND allowed region is fully explored in both cases.

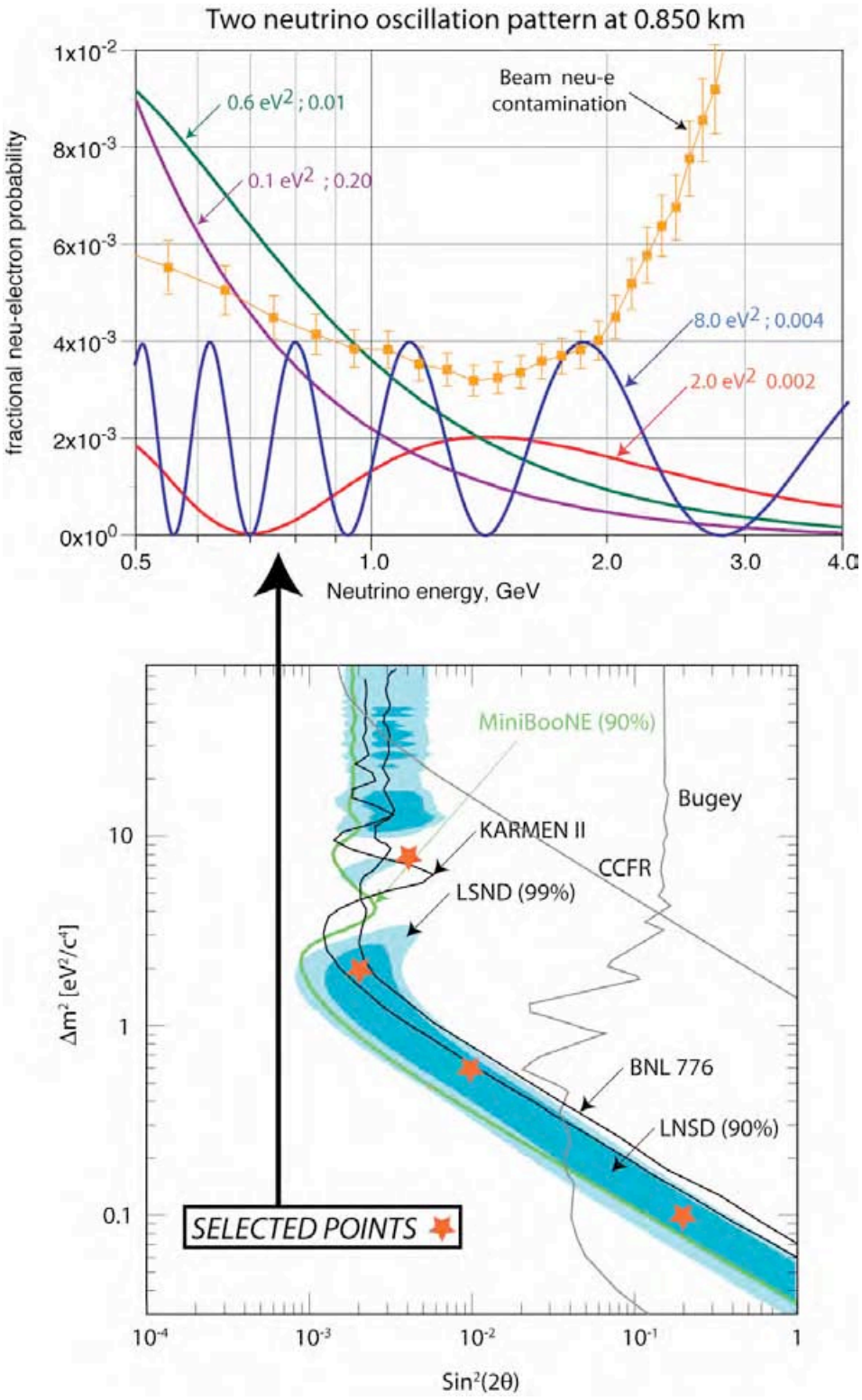


**Figure 28.** The experimentally expected oscillation patterns at 850 m shown for two neutrino oscillations and for some indicative positions of the LNSD allowed region (indicated with a star mark). The expected background due to the $\nu_e$ beam contamination is also indicated.

# 7 The realization of the detectors at the CERN/PS.

*7.1 General considerations.*

The detector in the CERN PS consists primarily in the "Near" and "Far" cryogenic detectors to be installed in the already existing Halls B-181 and B-191, where no major modification of the civil engineering are required since both Halls are already adequately instrumented. The three main fields of activities, i.e. (a) the CERN-PS beam line refurbishing, (b) the construction of the "Near" detector and (c) the modifications and T600 transfer from LNGS to CERN and can proceed independently without interferences from each other. These additional activities appear to be feasible in about two/three years.

The T600 has been already extensively operated on surface in Pavia during 2001. No limitation due to the higher cosmic ray backgrounds has been observed. Indeed the presently foreseen surface operation, including safety considerations, has been demonstrated to be much easier than the present underground operation in Hall B of the LNGS.

If the experiment is approved early in 2011, we are confident that useful data could be collected starting around the end of 2013, accounting also for the of beam and detectors commissioning, in time for the restart of PS operation after the long CERN accelerator shut down.

*7.2 Refurbishing of the T600 in the CERN-PS.*

The T600 is now presently perfectly operational in the underground Hall B, collecting data as CNGS2 experiment. The transport of the inner components of the detectors inside the main cryogenic boxes — 3,9 x 3,6 x 19,8 $m^3$, well under the crane capacity (40 ton), originally constructed in Pavia and previously transported to LNGS — is compatible with doors and obstacles. The internal detector will be therefore extracted fully assembled from cryostats with an existing, appropriate tooling and introduced in an appropriate container. The transport the other related components associated to cryogenics and electronics have been analyzed in detail and appear as entirely feasible.

The main modifications required in the hardware are a new external passive insulation which will be realized following the same technique to be adopted for the "Near" detector and a new, more efficient UV sensitive photomultipliers for trigger of the light collection from the LAr. The reinstallation of the TPC's into the new dewar allows the easy replacement of the light detection system with new generation 8 inches PMT's.

The structure of the cryogenic insulation can be realized with 1 m perlite walls on the four sides and on the top, while the bottom wall is realized with low conductivity bricks, also about 1 m thick. The specific heat loss is estimated to be about 5.8 W/m$^2$ for a nominal thermal conductivity of 0.029 W/m/K and a thickness of 1 m. Alternatively layers of readily available Divinycell H material, with a thermal conductivity of 0.030 W/m/K, can be used with an equivalent performance.

The over all cold surface of T600 is about 570 m$^2$, corresponding to a heat loss of ~ 3.3 kW. The improved insulation should allow to run the detector with only four active T600 cryo-cooler units (16 kW cold power), leaving the remaining eight existing cryo-cooler units for the "Near" detector and for additional cryogenic capacity of the system. Therefore no additional cryogenic capacity should be necessary for the installation of the whole new detector at CERN.

The T600 transfer operation can start during 2012 with the CERN site preparation, including ancillary equipments and the external holding structures. The detector can be dismounted and transported starting at the end of 2012, after having accomplished the CNGS2 physics run at LNGS.

As a guideline, a first estimate of the cost for the installation of the T600 in k€ are given in Table 6.

***Table 6.*** *Modification costs for "Far" detector in CERN-PS*

| **Item** | | **Cost in k€** |
|---|---|---|
| Dewar with passive insulation | | 2150 |
| *Engineering design and cryostat construction* | *2000* | |
| *Refurbishing of control process* | *50* | |
| *Chemical purifiers replacements* | *100* | |
| Transfer of T600 from LNGS to CERN | | 500 |
| *Dismantling and transport* | *250* | |
| *Reinstallation of TPC's into new dewar* | *250* | |
| Light collecting photomultipliers (PM) | | 480 |
| *PM's associated hardware* | *400* | |
| *Construction and commissioning* | *80* | |
| Final installation in the CERN-PS | | 300 |
| Contingency and miscellanea (20%) | | 680 |
| Income taxes (20%) | | 822 |
| **Total (k€)** | | **4932** |

*7.3 The new "Near" detector.*

Six months of additional studies are required for further simulations and laboratory investigations, in order to finalize the design of the "Near" detector.

The construction of the T600 inner detector— as described in the previous chapter — was realized in Italy by the CINEL Company, which would

be prepared to produce also the inner "Near" detector as a "clone" of the T600 geometry. This solution would permit the use of the same wire chambers mechanics and wiring infrastructures with a well determined cost and a relatively short time schedule.

The mechanical structures, including the wire frames, already described in detail in section 3.3 and the HV field cage (shaping rings and cathode) can be inserted in the containing cryogenic vessel as a single body. They will be built at the Company location and transported at CERN for final installation into the cryogenic vessel.

The additional 14200 read-out electronic channels will be built by industry following the existing T600 design. In analogy with the "Far" detector, the photomultipliers for the trigger signal will be based on the new design and 8 inches PMT's.

The over all cold surface of T150 is about 180 $m^2$, corresponding to a loss of 1.05 kW. This new passive insulation approach allows reducing the overall cryogenic consumption to a level manageable with a pair of T600 cryo-cooler units (8 kW cold power).

***Table 7.*** *Construction costs for "Near" detector in CERN-PS*

| **Item** | | **Cost in k€** |
|---|---|---|
| Dewar with passive insulation | | 750 |
| *Engineering design, cryostat construction* | *500* | |
| *Control process* | *75* | |
| *Chemical purifiers, including the pump systems* | *175* | |
| Wire planes and electron signal collecting structures | | 1700 |
| *Engineering design* | *170* | |
| *Wire chambers construction and commissioning* | *1380* | |
| *Race-track and cathode structures* | *150* | |
| H.V. supply for 150 kV feed-through | | 40 |
| *Engineering design* | *10* | |
| *Construction and commissioning* | *30* | |
| Light collecting photomultipliers | | 120 |
| *Costs of 30 PM and associated hardware* | *100* | |
| *Construction and commissioning* | *20* | |
| Readout electronics (3 mm pitch) | | 1350 |
| *Development costs* | *50* | |
| *Construction + commissioning of 14200 channels* | *1300* | |
| Final installation in the CERN-PS near site | | 200 |
| Liquid Argon for detector filling (200 t) | | 200 |
| Contingency and miscellanea (20%) | | 872 |
| Income taxes (20%) | | 1046.4 |
| **Total (k€)** | | **6278.4** |

# 8 References


[1] K. Nakamura et al., (Particle Data Group), J. Phys. G 37, 075021 (2010).

[2] B. Pontecorvo, Zh. Eksp. Teor. Fiz. 53, 1717 (1967) [Sov. Phys. JETP 26, 984 (1968)].

[3] G. Mention et al. arXiv:1101.2755v1 [hep-ex] and previous references therein.

[4] J. N. Abdurashitov et al. (SAGE Collaboration), Phys. Rev. C 80, 015807 (2009).

J. N. Abdurashitov et al. (SAGE Collaboration), Phys. Rev. Lett. 77, 4708 (1996).

J. N. Abdurashitov et al. (SAGE Collaboration), Phys. Rev. C 59, 2246 (1999).

J. N. Abdurashitov et al., Phys. Rev. C 73, 045805 (2006).

[5] F. Kaether, W. Hampel, G. Heusser, J. Kiko, and T. Kirsten, Phys. Lett. B 685, 47 (2010).

P. Anselmann et al. (GALLEX Collaboration), Phys. Lett. B 342, 440 (1995).

W. Hampel et al. (GALLEX Collaboration), Phys. Lett. B 420, 114 (1998).

[6] A. Aguilar et al. (LSND Collaboration), Phys. Rev. D 64, 112007 (2001).

[7] A. A. Aguilar-Arevalo (MiniBooNE Collaboration), Phys. Rev. Lett. 102, 101802 (2009).

A. A. Aguilar-Arevalo et al. (MiniBooNE Collaboration), arXiv:1007.1150.

[8] F.Mills, ICHEP, July 2010.

R. Van de Water, Neutrino 2010, Athens, Greece.

[9] C. Giunti, M. Laveder, Phys. Rev. D82 (2010) 053005 and previous references therein.

[10] E. Komatsu et al., arxiv.org/abs/1001.4538.

J. Dunkley et al., arxiv.org/abs/1009.0866.

J. Hamann et al. , arxiv.org/abs/1006.5276.

Y. I. Izotov, T. X. Thuan, arxiv.org/abs/1001.4440.

[11] C. Rubbia, CERN-EP/77-08 (1977).

A.Guglielmi, Neutrino 2010, Athens, Greece.

M. Antonello et al. , Paper in progress (2011).

[12] B. Baibussinov et al. , arXiv:0909.0355v3

[13] J. N. Bahcall, Phys. Rev. C 56, 3391 (1997).

[14] P. Vahle, Neutrino 2010, Athens, Greece.

[15] M. Guler et al., CERN-SPSC/99-26, SPSC/P311, 1999.

[16] V. N. Gavrin et al. arXiv:1006.2103.

[17] A. Ianni , D. Montanino, G. Scioscia, Eur. Phys. J. C8 (1999) 609-617.

[18] A. Porta et al., J. Phys. Conf. Ser. 203 012092 (2010).

IAEA Final Report: Focused Workshop on Antineutrino Detection for Safeguards Applications (2008).

[19] H. Chen et al., MicroBooNE, FNAL Proposal (2007) and Addendum (2008).

[20] I. Stancu et al., OscSNS [http://physics.calumet.purdue.edu/~oscsns] White Paper (2008).

[21] ICARUS Coll., ICARUS initial physics program, ICARUS-TM/2001-03 LNGS P28/01 LNGS-EXP 13/89 add.1/01; ICARUS Coll., Cloning of T600 modules to reach the design sensitive mass, ICARUS-TM/2001-08 LNGS-EXP 13/89 add.2/01.

[22] F. Arneodo et al., Phys. Rev. D 74 (2006) 112001.

[23] S. Amoruso et al., Nucl. Instrum. Meth. A 523 (2004), 275; S. Amoruso et al., Nucl. Instrum. Meth. A 516 (2004) 68.

[24] G. Charpak et al., Nucl. Instrum. and Meth. 80, (1970), 13.

[25] B. Baibussinov et al., JINST **5** P03005 (2010).

[26] B. Baibussinov et al., Astr. Part. Phys. J. 29 (2008) 174-187; D. Angeli et al., JINST **4** P02003 (2009).

[27] S. Amerio et al., Nucl. Instr. And Meth. A527 (2004) 329.

[28] M. Baldo-Ceolin et al., CERN/PSCC/80-130, PSCC/P33, 30-10-1980; C. Angelini et al. [PS180 Coll.], Phys. Lett. B 179 (1986) 307.

[29] R.L.Aguiar et al, CERN nTOP Facility, CERN/INTC 2000-016, INTC/P123 (2000).

[30] Information on CERN-PS neutrino beam refurbishing project available at: http://info-psnf.web.cern.ch/info-PSNF/Presentations.

[31] A. Ankowski et al., Eur. Phys. J. C48 (2006) 667; K. Cieslik et al., ICARUS-TM/07-02 (2007).

[32] S. Amoruso et al., Eur. Phys. J. C33 (2004) 233.

[33] A. Ankowsky et al., Acta Phys. Pol. B 41 vol. 1 (2010) 103.

[34] J. Altegoer et al., Nucl. Instr. And Meth. A404 (1998) 96; P. Astier et al., Nucl. Instr. And Meth. A515 (2003) 800; J. Altegoer et al., Nucl. Instr. And Meth. A428 (1999) 299.

[35] G. Battistoni et al., "The FLUKA code: Description and benchmarking", AIP Conf. Proc. 896, 31-49, (2007); G. Battistoni et al., A neutrino-nucleon interaction generator for the FLUKA Monte Carlo code, Pro-

ceedings of the 12th International conference on nuclear reaction mechanisms, Varenna (Italy), June 15 - 19, 2009, p.307; Ferrari et al., FLUKA, a multi particle transport code (program version 2005), CERN-2005-10, INFN/TC-05/11, 2005.

[36] G. Battistoni et al., Acta Phys. Polon. B37 (2006) 2361.

[37] G.P. Zeller, Neutrino Cross Sections: Past, Present and Future, talk at NuInt07, FNAL (2007) [http://theory.fnal.gov/jetp/talks/zeller.pdf]; G.P. Zeller, Low Energy Neutrino Cross Sections: Comparison of various Monte Carlo Predictions to Experimental Data, talk at NuINt02 Irvine (2002) [hep-ph/0312061v1].